

Efficient Time-Series Approximation with Linear Recurrent Neural Networks: Architecture Learning and Predictive Power

The Power of Linear Recurrent Neural Networks

Frieder Stolzenburg^{1*}, Sandra Litz¹, Olivia Michael², Oliver Obst²

¹Faculty of Automation and Computer Sciences, Harz University of Applied Sciences, Friedrichstr. 57-59, 38855 Wernigerode, Germany.

²Centre for Research in Mathematics and Data Science, Western Sydney University, Locked Bag 1797, Penrith NSW 2751, Australia.

*Corresponding author(s). E-mail(s): fstolzenburg@hs-harz.de;
 Contributing authors: litz_sandra@web.de; olivia_michael@hotmail.com;
o.obst@westernsydney.edu.au;

Abstract

Recurrent neural networks are a powerful means to cope with time series. We show how autoregressive linear, i.e., linearly activated recurrent neural networks (LRNNs) can approximate any time-dependent function $f(t)$. The approximation can effectively be learned by simply solving a linear equation system; no backpropagation or similar methods are needed. Furthermore, and this is the main contribution of this paper, the size of an LRNN can be reduced significantly in one step after inspecting the spectrum of the network transition matrix, i.e., its eigenvalues, by taking only the most relevant components. Therefore, in contrast to other approaches, we do not only learn network weights but also the network architecture. LRNNs have interesting properties: They end up in ellipse trajectories in the long run and allow the prediction of further values and compact representations of functions. We demonstrate this by several case studies, among them multiple superimposed oscillators (MSO), robotic soccer (RoboCup), and stock price prediction. LRNNs outperform the previous state-of-the-art for the MSO task with a minimal number of units.

Keywords: recurrent neural network, linear activation, time-series analysis, prediction, dimensionality reduction, approximation theorem, ellipse trajectories

1 Introduction

Deep learning generally refers to a class of machine learning algorithms that use a cascade of multiple layers of nonlinear processing units for feature extraction and transformation [1]. The tremendous success of deep learning in diverse fields of artificial intelligence, such as computer vision and natural language processing, appears to depend on several key components: artificial, possibly recurrent neural networks (RNNs) with nonlinearly activated neurons, convolutional

layers, and iterative training methods such as backpropagation [2]. However, which of these components are truly essential for machine learning tasks such as time-series analysis?

Research in time-series analysis and hence the modeling dynamics of complex systems has a long tradition and remains highly active due to its crucial role in many real-world applications [3], such as weather forecasts, stock quotations, comprehension of trajectories of objects and agents, and solving number puzzles [4, 5]. Among other benefits, the analysis of time series enables data compression, i.e., the compact representation of time series, by a function $f(t)$, and prediction of future values.

Numerous studies address these topics using RNNs, particularly variants of networks with long short-term memory (LSTM) [6]. Recent works in this area also aim to enhance the performance of RNNs, e.g., HiPPO [7] and structured state spaces [8, 9], which learn representations of signals over time. There are also more biologically inspired spiking neural networks [10] that can perform (simple) delay tasks quite well.

In the following, we consider an alternative, yet simple but very powerful type of RNNs: linear recurrent neural networks (LRNNs). We utilize linear activation, which allows us to minimize the network size in one step by inspecting the eigenvalues of the network transition matrix (cf. Section 4.3). Unlike other approaches, we do not only learn network weights but also the network architecture itself. LRNNs are a computationally efficient complement to more demanding approaches, suitable for scenarios where simplicity and rapid deployment are crucial.

The rest of this paper is structured as follows: First, we briefly review related works (Section 2). We then formally introduce LRNNs as a special and simple kind of RNNs together with their properties, including the general network dynamics and their long-term behavior (Section 3). Afterwards, learning LRNNs is explained (Section 4). It is a relatively straightforward procedure that allows network size reduction; no backpropagation or gradient-descent method is needed. We then discuss results and experiments (Section 5), before concluding with our findings (Section 6).

Interestingly, many results for LRNNs presented here can be achieved by applying linear algebra and matrix analysis. Our theoretical contributions facilitate a highly efficient learning process, previously unexplored in the literature. Our approach allows for significant reductions in network size directly after initial training (cf. Section 4). In addition, the empirical evaluations, particularly of the MSO benchmark and stock price prediction (cf. Sections 5.1 and 5.4) with LRNNs and other approaches, such as LSTM networks, demonstrate the practical applicability of our approach. We are confident that this work will serve as a valuable resource across various domains, including neural engineering, time series prediction, and echo state networks.

2 Related Works

2.1 Echo State Networks

Echo state networks (ESNs) [11, 12] play a significant role in RNN research as they provide an architecture and supervised learning principle for RNNs. They do this by driving a random, large, fixed RNN, called *reservoir*, with the input signal which then induces in each neuron within this reservoir network a nonlinear response signal. They combine a desired output signal with a trainable linear combination of all response signals, allowing dimensionality reduction by so-called *conceptors* [13, 14].

One variant of ESNs combines several independent (decoupled) smaller networks [15]. ESN-style (random) initialization has been shown effective for training RNNs with Hessian-free optimization [16]. The latter paper addresses the problem of how to effectively train recurrent neural networks on complex and difficult sequence modeling problems which may contain long-term data dependencies. This can also be done with LRNNs (cf. MSO benchmark, Section 5.1). Previous work in [17] considers the effect of weight changes in linear symmetric ESNs on (Fisher) memory of the network. Furthermore, Couillet et al. [18] investigate the asymptotic performance of linear ESNs from a solely theoretical point of view.

2.2 Recurrent Neural Networks

Simple RNNs have been proposed originally by Elman [19]. By allowing them to accept sequences as inputs and outputs rather than individual observations, RNNs extend the standard feedforward multilayer perceptron networks. As shown in many sequence modeling tasks, data points such as video frames, audio snippets, and sentence segments are usually highly related in time. This results in RNNs being used as the indispensable tools for modeling such temporal dependencies. Linear RNNs and some of their properties (such as short-term memory) are already investigated in [20]. Unfortunately, however, it can be a struggle to train RNNs to capture long-term dependencies [21, 22]. This is due to the gradients vanishing or exploding during backpropagation which in turn makes the gradient-based optimization difficult.

As a next step, long short-term memory (LSTM) networks [6] became a prominent and dominant type of RNN. The expression *long short-term* refers to the fact that LSTM is a model for the short-term memory which can last for a long period of time. An LSTM is well-suited to classify, process and predict time series given time lags of unknown size. They were developed to deal with the exploding and vanishing gradient problem when training traditional RNNs. A common LSTM unit is composed of a cell, an input gate, an output gate, and a forget gate. Each unit type is activated in a different manner, whereas in this paper we consider completely linearly activated RNNs.

State-frequency memory (SFM) RNNs [23] aim to model the frequency patterns of the temporal sequences. The key idea of the SFM is to decompose the memory states into different frequency states. In doing so, they can explicitly learn the dependencies of both the low and high frequency patterns. As we will see (cf. Section 5.1), RNNs in general can easily learn time series that have a constant frequency spectrum, which may be obtained also by Fourier analysis.

The NoBackTrack algorithm [24] trains RNN parameters in an online, memoryless setting which therefore requires no backpropagation through time. It is also scalable, thus avoiding the large computational and memory cost of maintaining the full gradient of the current state with respect to the parameters, but it still uses an iterative method, namely gradient descent. In contrast to this and other related works, in this paper we present a method working with linearly activated RNNs that does not require backpropagation or similar procedures in the learning phase. Nevertheless, for feedforward neural networks, the forward-forward algorithm [25] presents an approach to training models without backpropagation but, at least in its current form, is only applicable to the classification of static patterns.

The Legendre memory unit (LMU) [26] is a memory cell for recurrent neural networks that maintains information across long windows of time using relatively few resources. It is derived from the linear transfer function for a continuous-time history of its input signal across a sliding window, approximated by coupled differential equations, which can implicitly also be solved by LRNNs (cf. Property 1). Carta et al. [27] propose an approach to address memorization challenges in RNNs which puts forward a way between the random encoding in the reservoir paradigm and the vanishing-gradient prone approach of fully-trained RNNs. The objective is to train memorization units to maximize their short-term memory capacity, employing a linear autoencoder for sequences. More recently, deep state-space models have been shown to perform well on long sequence modeling tasks. Gu et al. [8] and Orvieto et al. [28] cover ideas of linear recurrent equations in so-called state spaces, Jordan-type factorizations, and links to continuous-time differential equations. Nevertheless, in all these cases, backpropagation is employed, which is not needed for LRNNs whose network size is reduced significantly in addition (cf. Section 4.3), thus we address the topic of architecture learning.

Architecture learning, in particular the pruning of neural networks, has been studied extensively in the literature, with an early survey on pruning algorithms for neural networks in [29]. More recently, Lee et al. [30] present a method that prunes irrelevant connections between neurons for a given task prior to training and is applicable to a variety of modern neural network models, resulting in sparse networks. Furthermore, Molchanov et al. [31] propose a method that estimates the contribution of a neuron to the final loss and iteratively removes

those with smaller scores. In contrast to this, for LRNNs, the network architecture and hence its size are reduced in one step by analyzing the network transition matrix (cf. Section 4.3).

In more recent works, linear RNNs are considered explicitly: Zhang et al. [32] establish an explicit connection and a direct architectural match between Koopman operator approximation and linear RNNs, with the goal of time-series prediction. Durstewitz [33] considers piecewise linear RNNs and develops a specific maximum-likelihood estimation scheme for them. Furthermore, Fan et al. [34] investigate block-diagonal, input-dependent, linear RNNs, exploring them in the context of regular language modeling. However, none of these recent works consider network size reduction as done here.

2.3 Autoregression

An *autoregressive model* is a representation of a type of random process [35]. It specifies that the output variable or a vector thereof depends linearly on its own predecessor values and on a stochastic term (white noise). In consequence, the model is in the form of a stochastic differential equation as in general (physical) dynamic systems [36]. An LRNN is also linearly activated, but its output does not only depend on its own predecessor values and possibly white noise but on the complete state of the possibly big reservoir whose dynamics is explicitly dealt with. In addition, the size of the network might be reduced in the subsequent process. We will continue the comparison between autoregression and LRNNs later (cf. Section 4.1), as we mainly consider autoregressive tasks in the following.

A popular choice in this context is the autoregressive integrated moving average (ARIMA) model [37, 38]. A standard ARIMA(p, d, q) model consists of autoregression AR(p) and a moving average MA(q). The parameter p describes the history length (lag order) used to predict the time series at time t . We have $f(t) = c_1 f(t-1) + \dots + c_p f(t-p) + e_t$ where c_1, \dots, c_p are (real-valued) autocorrelation coefficients and e_t , the residuals, is Gaussian white noise. In the moving average process MA(q), the value q specifies the number of past residuals considered for prediction. An underlying trend of the time series is modeled by using a drift, i.e., a constant that extends the term. This procedure is particularly well-suited for stationary time series, i.e., whose properties do not vary with time. Many time series, however, exhibit non-stationary behavior and thus require a transformation to make them stationary. This is achieved by investigating the derivatives of the series, with the order of this process given by the parameter d .

State-space time series models, which are a natural bridge between autoregressive models and LRNNs, have been studied at length [39]. Autoregressive frameworks are also common in current machine-learning applications such as large language models (LLMs), e.g., in the generative pre-trained transformer GPT-3, GPT-4 and related models, by next word prediction [40, 41]. The models applied in this context, however, are very complex (175 billion parameters and much more) and nonlinear. Related to autoregression is autoencoding of sequences. It has been shown in [42] that linear autoencoders can be used for pre-training of RNNs, while we establish completely linear RNNs here. Furthermore, [43] gives an exact closed-form solution for the weights of the linear autoencoder, which is related to the approximation theorem for LRNNs (cf. Property 8).

3 Linear Recurrent Neural Networks

RNNs often host several types of neurons, each activated in a different manner [19, 6]. In contrast, we understand a homogeneous interconnected group of standard neurons simply as a (recurrent) neural network here, which may have arbitrary loops, akin to biological neuronal networks. We adopt a *discrete time model*, that is, the input and output are represented by a time series and are processed synchronously and stepwise by the network.

Definition 1 (time series). A *time series* is a series of data points in d dimensions $S(0), \dots, S(n) \in \mathbb{R}^d$ with $d \geq 1$ and $n \geq 0$.

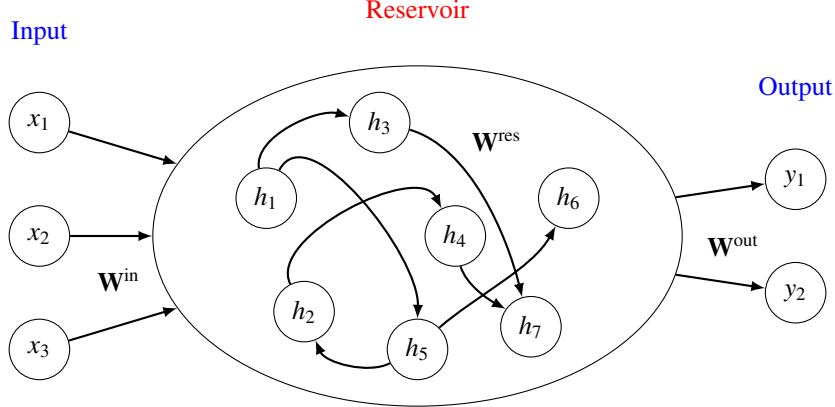


Figure 1 General recurrent neural network. In ESNs, only output weights are trained and the hidden layer is also called reservoir.

Definition 2 (recurrent neural network). A *recurrent neural network* (RNN) is a directed graph consisting of altogether N nodes, called *neurons*. $x(t)$ denotes the *activation* of the neuron x at (discrete) time t . We may distinguish three groups of neurons (cf. Figure 1):

- N^{in} *input* neurons (usually without incoming edges) whose activation is given by an external source, e.g., a time series,
- N^{out} *output* neurons (usually without outgoing edges) whose activation represents some output function, and
- N^{res} *reservoir* or *hidden* neurons (arbitrarily connected) that are used for auxiliary computations.

The sets of input and output neurons are not necessarily disjoint, they may even be identical (cf. Definition 3). Therefore, in the following, let N^{inout} denote the overall number of neurons in the union of both sets. Obviously it holds $N = N^{\text{inout}} + N^{\text{res}}$ and $N^{\text{inout}} \leq N^{\text{in}} + N^{\text{out}}$.

The edges of the directed graph represent the network connections. They are annotated with *weights* which are compiled into the *transition matrix* W of size $N \times N$. An entry w_{ij} in row i and column j denotes the weight of the edge from neuron j to neuron i . If there is no connection, then $w_{ij} = 0$. The transition matrix has the form

$$W = \begin{bmatrix} W^{\text{out}} \\ W^{\text{in}} \quad W^{\text{res}} \end{bmatrix} \quad (1)$$

containing the following weight matrices:

- *input* weights W^{in} (weights from the input and possibly the output to the reservoir, a matrix of size $N^{\text{res}} \times N^{\text{inout}}$),
- *output* weights W^{out} (all weights to the output and possibly back to the input, a matrix of size $N^{\text{inout}} \times N$), and
- *reservoir* weights W^{res} (weights within the reservoir, a matrix of size $N^{\text{res}} \times N^{\text{res}}$).

Let us now define the *network activity*: The initial configuration of the neural network is given by a column vector s with N components, called *start vector*. It represents the network state at the start time $t = t_0$. Because of the discrete time model, the activation of a (non-input) neuron x_i at time $t + \tau$ (for some time step $\tau > 0$) from the activation at time t of the neurons x_1, \dots, x_k (for some $k \geq 0$), connected to x_i with the weights w_{i1}, \dots, w_{ik} , is computed as follows:

$$x_i(t + \tau) = g(w_{i1}x_1(t) + \dots + w_{ik}x_k(t)) \quad (2)$$

This has to be done simultaneously for all neurons of the network. g is called *activation function*. Although we will not make use of it, g may be different for different parts of the network. Usually, a nonlinear, bounded, strictly increasing, sigmoidal function g is used, e.g., the logistic function, the hyperbolic tangent (tanh), or the softplus function [2, Section 3.10].

In the following, we employ simply the (linear) identity function, i.e., $g(x) = x$ for all x , and can still approximate arbitrary time-dependent functions (cf. Property 8).

Definition 3 (linear recurrent neural network). A *linear recurrent neural network* (LRNN) is an RNN with the following properties:

1. For the start time, it holds that $t_0 = 0$ and τ is constant, usually $\tau = 1$.
2. The initial state $S(0)$ of the given time series constitutes the first d components of the start vector s .
3. For all neurons we have *linear activation*, i.e., everywhere g is the identity.
4. The weights in W^{in} and W^{res} are taken randomly, independently, and identically distributed from the standard normal distribution, i.e., the Gaussian distribution with mean $\mu = 0$ and standard deviation $\sigma = 1$, and remain unchanged all the time, whereas the output weights W^{out} are learned (cf. Section 4.1).
5. The spectral radius of the reservoir weights matrix W^{res} is set to 1, i.e., W^{res} is divided by the maximal absolute value of all its eigenvalues. Note that the spectral radius of the overall transition matrix W (cf. Equation 1) may still be greater than 1 if required by the application (cf. Example 4).
6. There is no distinction between input and output but only one (joint) group of $N^{\text{inout}} = N^{\text{in}} = N^{\text{out}} = d$ input/output neurons. They may be arbitrarily connected like the reservoir neurons. We thus can imagine the whole network as a big reservoir because the input/output neurons are not particularly special.

LRNNs can run in one of two *modes*: either receiving input or generating (i.e., predicting) output. In output generating mode, the network runs autonomously, thus without external input. In this case, Equation 2 is applied to all neurons including the input/output neurons. The output from the previous time step is copied to the input. In input receiving mode, the activation of every input/output neuron x at time t is always overwritten with the respective input value at time t given by the time series S .

3.1 Examples

Example 1. The function $f(t) = t^2$ can be realized by an LRNN (in output generating mode) with three neurons (cf. Figure 2(a)). The respective transition matrix W and start vector s are:

$$W = \begin{bmatrix} 1 & 2 & 1 \\ 0 & 1 & 1 \\ 0 & 0 & 1 \end{bmatrix} \text{ and } s = \begin{bmatrix} 0 \\ 0 \\ 1 \end{bmatrix}$$

Consequently, starting at $t = 0$ with time step $\tau = 1$, we have:

- $x_3(0) = 1, x_3(t+1) = x_3(t)$, and hence $x_3(t) = 1$ in general.
- $x_2(0) = 0, x_2(t+1) = x_2(t) + x_3(t) = x_2(t) + 1$, and hence $x_2(t) = t$.
- $x_1(0) = 0, x_1(t+1) = x_1(t) + 2x_2(t) + x_3(t) = x_1(t) + 2t + 1$, and hence $x_1(t) = t^2$ because of the identity $(t+1)^2 = t^2 + 2t + 1$ (cf. first row of the transition matrix W).

Thus, in the neuron x_1 , the function $f(t)$ is computed. It is the only input/output neuron in this case.

Example 2. The Fibonacci series $(0, 1, 1, 2, 3, 5, 8, \dots)$ can be defined as follows:

$$f(t) = \begin{cases} t, & \text{for } t = 0, 1 \\ f(t-1) + f(t-2), & \text{otherwise} \end{cases}$$

It can be realized by an LRNN (in output generating mode) with just two neurons (cf. Figure 2(b)). The respective transition matrix W and start vector s can be directly derived from the recursive definition of f :

$$W = \begin{bmatrix} 0 & 1 \\ 1 & 1 \end{bmatrix} \text{ and } s = \begin{bmatrix} 0 \\ 1 \end{bmatrix}$$

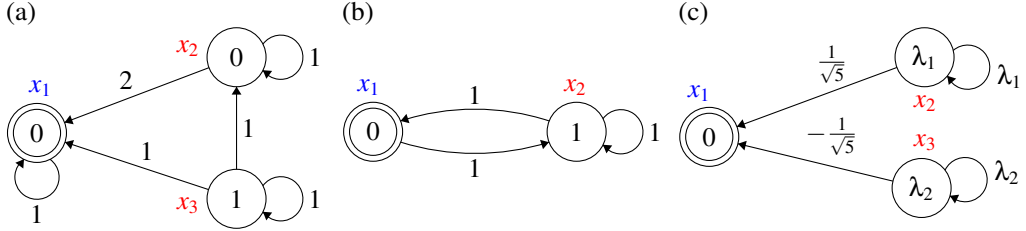


Figure 2 LRNNs for (a) $f(t) = t^2$ and (b+c) the Fibonacci series (0, 1, 1, 2, 3, 5, 8, ...) with time step $\tau = 1$. In each case, the input/output neuron x_1 is marked by a double circle. The initial values of the neurons at time $t_0 = 0$ are written in the nodes. The weights are annotated at the edges.

Again, the function $f(t)$ is computed in the only input/output neuron x_1 . In the other neuron x_2 , $f(t+1)$ is generated. There is a closed-form expression for the Fibonacci series, revealing its exponential growth, known as *Binet's formula*:

$$f(t) = \frac{\lambda_1^t - \lambda_2^t}{\sqrt{5}} \text{ with } \lambda_1 = \frac{1 + \sqrt{5}}{2} \approx 1.61803 \text{ (golden ratio) and } \lambda_2 = 1 - \lambda_1 \quad (3)$$

Interestingly, λ_1 and λ_2 are the eigenvalues of the above transition matrix W . Moreover, Binet's formula can be used to create another LRNN to calculate the Fibonacci series (cf. Figure 2(c)). We will come back to this later (in Example 4).

Property 1. LRNNs are well suited to represent differential equations and to solve them numerically. To see this, consider the homogeneous linear differential equation

$$\sum_{k=0}^n c_k x^{(k)}(t) = 0 \quad (4)$$

where $c_k \in \mathbb{R}$ are constant coefficients with $c_n \neq 0$, $x^{(k)}(t)$ is the k -th derivative of the function x with respect to time t , and $n > 0$. It can be solved approximately by LRNNs with start vector s satisfying Equation 4 and the following transition matrix:

$$W = \begin{bmatrix} 1 & \tau & 0 & \cdots & 0 \\ 0 & 1 & \tau & \ddots & 0 \\ \vdots & \ddots & \ddots & \ddots & 0 \\ 0 & \cdots & 0 & 1 & \tau \\ 0 & -\tau \frac{c_0}{c_n} & \cdots & -\tau \frac{c_{n-2}}{c_n} & 1 - \tau \frac{c_{n-1}}{c_n} \end{bmatrix} \quad (5)$$

Proof. See Section A. □

Example 3. The exponential function $\exp(t) = e^t$ can be defined by the differential equation $\dot{x}(t) = x(t)$, i.e., we have $c_0 = 1$ and $c_1 = -1$ in Equation 4. In consequence, according to Property 1 and because of $\exp(0) = \exp(0) = 1$, the transition matrix W and start vector s of the corresponding LRNN are:

$$W = \begin{bmatrix} 1 & \tau \\ 0 & 1 + \tau \end{bmatrix} \text{ and } s = \begin{bmatrix} 1 \\ 1 \end{bmatrix}$$

Induction over time yields immediately $x(t) = \dot{x}(t) = (1 + \tau)^{t/\tau} \approx e^t$ for small $\tau > 0$ (according to Euler) as expected.

The strong relationship between RNNs and differential equations is already known [44, Section 9] as well as the extraction of eigenvalues to describe dynamical systems [45, Section 5]. Nevertheless, as we will show in the rest of this paper, the combination of both provides an effective method for network size reduction (cf. Section 4.3) and therefore seems to be worthwhile to be considered by the machine learning community in more detail.

3.2 Network Dynamics

An LRNN runs through network states $f(t)$ for $t \geq 0$. It holds (in output generating mode)

$$f(t) = \begin{cases} s, & t = 0 \\ W \cdot f(t - \tau), & \text{otherwise} \end{cases}$$

and hence simply $f(t) = W^t \cdot s$ for $\tau = 1$ (cf. Definition 3).

Property 2. Let $W = V \cdot J \cdot V^{-1}$ be the Jordan decomposition of the transition matrix W where J is the direct sum of one or more Jordan blocks, i.e., a block diagonal matrix formed of Jordan blocks

$$J_m(\lambda) = \begin{bmatrix} \lambda & 1 & 0 & \cdots & 0 \\ 0 & \lambda & 1 & \ddots & \vdots \\ \vdots & \ddots & \ddots & \ddots & 0 \\ \vdots & & \ddots & \lambda & 1 \\ 0 & \cdots & \cdots & 0 & \lambda \end{bmatrix}$$

in general with different sizes $m \times m$ and different eigenvalues λ , and V is a matrix consisting of the corresponding eigen- and principal column vectors. Then we have:

$$f(t) = W^t \cdot s = V \cdot J^t \cdot V^{-1} \cdot s$$

If we decompose V into matrices v of size $N \times m$ and the column vector $V^{-1} \cdot s$ into a stack of column vectors w of size m , corresponding to the Jordan blocks in J , then $f(t)$ can be expressed as a sum of vectors $u = v \cdot J_m(\lambda)^t \cdot w$ where the Jordan block powers are upper triangular Toeplitz matrices, i.e., in which each descending diagonal from left to right is constant, with:

$$(J_m(\lambda)^t)_{ij} = \binom{t}{j-i} \lambda^{t-(j-i)} \quad [46, \text{Section 3.2.5}] \quad (6)$$

Remark 1. Although the parameter t is discrete, i.e., a nonnegative integer number, the values of $f(t) = W^t \cdot s$ can also be computed for $t \in \mathbb{R}$ and are always real. For this, we consider the Jordan block powers from Equation 6:

- The definition of the binomial coefficient $\binom{t}{k} = \frac{t(t-1)\cdots(t-k+1)}{k(k-1)\cdots 1}$ is applicable for real and even complex t and nonnegative integer k . For negative k , we have $\binom{t}{k} = 0$.
- For real matrices W , there are always complex conjugate eigenvalue pairs λ and $\bar{\lambda}$ and corresponding complex coefficients c and \bar{c} (resulting from the respective matrix u and vector v in Property 2). With $c = |c| e^{i\psi}$ and $\lambda = |\lambda| e^{i\omega}$, we get $c\lambda^t + \bar{c}\bar{\lambda}^t = |c||\lambda|^t \cos(\omega t + \psi)$ applying Euler's formula. This obviously is defined for all $t \in \mathbb{R}$ and always yields real-valued $f(t)$.
- Negative real eigenvalues, i.e., the case $\lambda < 0$, should be treated in a special way, namely by replacing λ^t by $|\lambda|^t \cos(\pi t)$. Both terms coincide for integer t , but only the latter is real-valued for all $t \in \mathbb{R}$. The powers of positive real eigenvalues λ are always positive and real and hence need no special consideration.

A Jordan decomposition exists for every square matrix W [46, Theorem 3.1.11]. But if W has N distinct eigenvectors, there is a simpler decomposition, called *eigendecomposition*. The transition matrix W is *diagonalizable* in this case, i.e., similar to a diagonal matrix D , and the network dynamics can be directly described by means of the eigenvalues and eigenvectors of W :

Property 3. Let $W = V \cdot D \cdot V^{-1}$ be the eigendecomposition of the transition matrix W with column eigenvectors v_1, \dots, v_N in V and corresponding eigenvalues $\lambda_1, \dots, \lambda_N$, on the diagonal of the diagonal matrix D , sorted in decreasing order with respect to their absolute values. Like every column vector, we can represent the start vector s as linear combination of the eigenvectors, namely as $s = x_1 v_1 + \cdots + x_N v_N = V \cdot x$ where $x = [x_1 \cdots x_N]^\top$ such that $x = V^{-1} \cdot s$. Since W is a linear mapping and for each eigenvector v_k with eigenvalue λ_k with $1 \leq k \leq N$

it holds that $W \cdot v_k = \lambda_k v_k$, we have $W \cdot s = W \cdot (x_1 v_1 + \dots + x_N v_N) = x_1 \lambda_1 v_1 + \dots + x_N \lambda_N v_N$. Induction over t yields immediately:

$$f(t) = W^t \cdot s = V \cdot D^t \cdot x = x_1 \lambda_1^t v_1 + \dots + x_N \lambda_N^t v_N \quad (7)$$

3.3 Real-Valued Transition Matrix Decomposition

For real-valued transition matrices W , it is possible to define a decomposition that, in contrast to the ordinary Jordan decomposition in Property 2, solely makes use of real-valued components, adopting the so-called *real Jordan canonical form* [46, Section 3.4.1] of the square matrix W (cf. Section B). But the subsequent theorem (Property 4) shows a more general way: The matrix V from Property 2 is transformed into a real matrix A and, what is more, the start vector s can be replaced by an arbitrary column vector y with all nonzero entries.

Property 4. Let $W = V \cdot J \cdot V^{-1}$ be the (real) Jordan decomposition of the transition matrix W and s the corresponding start vector. Then for all column vectors y of size N with all nonzero entries, there exists a square matrix A of size $N \times N$ such that for all $t \geq 0$ we have:

$$f(t) = W^t \cdot s = A \cdot J^t \cdot y$$

Proof. See Section C. □

3.4 Long-Term Behavior

Let us now investigate the long-term behavior of an LRNN (run in output generating mode) by understanding it as an (autonomous) *dynamic system* [36, 45]. We will see (in Property 6) that the network dynamics may be reduced to a very small number of dimensions/neurons in the long run. They determine the behavior for $t \rightarrow \infty$. Nevertheless, for smaller t , the use of many neurons is important for computing short-term predictions.

Property 5. In all of the N dimensions, $f(t) = W^t \cdot s$ grows only polynomially or single-exponentially in t .

Proof. See Section D. □

In fact, LRNNs can model polynomials (cf. Example 1, parabola), general single-exponential functions such as the Fibonacci series (cf. Example 2), multiple superimposed oscillators (cf. Example 6), and many more (cf. Property 8). For this, the overall transition matrix W may have (a) a spectral radius greater than 1 and (b) many eigenvalues (more than two) with absolute value 1. Nevertheless, it is interesting to investigate a special case, namely a *pure random reservoir* where both conditions do not hold:

Property 6. Consider an LRNN solely consisting of a random reservoir whose transition matrix W^{res} (a) is completely real-valued, (b) has an eigendecomposition $W^{\text{res}} = V \cdot D \cdot V^{-1}$ (as in Property 3) with unit spectral radius, and thus (c) all eigenvalues are distinct (which is almost always, i.e., with probability close to 1, true for random matrices), together with a completely real-valued random start vector s with unit norm. Then, almost all terms $x_k \lambda_k^t v_k$ in Equation 7 vanish for large t because for all eigenvalues λ_k with $|\lambda_k| < 1$ we have $\lim_{t \rightarrow \infty} \lambda_k^t = 0$.

Although a general real matrix can have more than two complex eigenvalues which are on the unit circle, for a pure random reservoir as considered here, almost always only the (largest) eigenvalues λ_1 and possibly λ_2 have the (maximal) absolute values 1. In consequence, we have one of the following cases:

1. $\lambda_1 = +1$. In this case, the network activity contracts to one point, i.e., to a *singularity*:

$$\lim_{t \rightarrow \infty} f(t) = x_1 v_1$$
2. $\lambda_1 = -1$. For large t it holds that $f(t) \approx x_1 (-1)^t v_1$. This means we have an *oscillation* in this case. The dynamic system alternates between the two points $\pm x_1 v_1$.
3. λ_1 and λ_2 are two (properly) complex eigenvalues with absolute value 1. Since W^{res} is a real-valued matrix, the two eigenvalues as well as the corresponding eigenvectors v_1 and

v_2 are complex conjugate with respect to each other. Thus, for large t , we have an *ellipse* trajectory

$$f(t) \approx x_1 \lambda_1^t v_1 + x_2 \lambda_2^t v_2 = \tilde{V} \cdot \tilde{D}^t \cdot \tilde{x}$$

where $\tilde{V} = [v_1 \ v_2]$, $\tilde{D} = \begin{bmatrix} \lambda_1 & 0 \\ 0 & \lambda_2 \end{bmatrix}$, and $\tilde{x} = \begin{bmatrix} x_1 \\ x_2 \end{bmatrix}$.

We can build a matrix \hat{D} , similar to \tilde{D} but completely real-valued (cf. Section 3.3) which states the ellipse rotation. Furthermore, the rotation speed can be derived from the eigenvalue λ_1 as follows: In each step of length τ , there is a rotation by the angle $\omega\tau$ where ω is the angular frequency, which can be determined from the equation $\lambda_1 = |\lambda_1| e^{i\omega\tau}$ (cf. Remark 1). The two-dimensional ellipse trajectory can be stated by two (co)sinusoids then: $f(t) = [a \cos(\omega t) \ b \sin(\omega t)]^\top$ where $a, b > 0$ are half the width and height of the ellipse. Applying the addition theorems of trigonometry, we get:

$$\begin{aligned} f(t + \tau) &= \begin{bmatrix} a \cos(\omega(t + \tau)) \\ b \sin(\omega(t + \tau)) \end{bmatrix} = \begin{bmatrix} a(\cos(\omega t)\cos(\omega\tau) - \sin(\omega t)\sin(\omega\tau)) \\ b(\sin(\omega t)\cos(\omega\tau) + \cos(\omega t)\sin(\omega\tau)) \end{bmatrix} \\ &= \underbrace{\begin{bmatrix} \cos(\omega\tau) & -a/b\sin(\omega\tau) \\ b/a\sin(\omega\tau) & \cos(\omega\tau) \end{bmatrix}}_{\hat{D}} \cdot f(t) \end{aligned}$$

From this, we can read off the desired ellipse rotation matrix \hat{D} as indicated above. Due to Property 4, there exists a (two-dimensional) start vector y and a transformation matrix A such that

$$f(t) \approx A \cdot \hat{D}^t \cdot y \quad (8)$$

for large t . Every LRNN with many neurons can thus be approximated by a simple network with at most two neurons. The output values lie on an ellipse in general, thus in only two dimensions. Nonetheless, in the beginning, i.e., for small t , the dynamics of the system is not that regular (cf. Figure 3). But although Property 6 states only the asymptotic behavior of random LRNNs with unit spectral radius, interestingly the network dynamics converges relatively fast to the final ellipse trajectory: The (Euclidean) distance between the actual value $f(t)$ (according to Equation 7) and its approximation by the final ellipse trajectory (Equation 8) is almost zero already after a few hundred steps (cf. Figure 4). Of course this depends on the eigenvalue distribution of the transition matrix [47]. So the long-term behavior may be different for transition matrices other than pure random reservoirs.

The long-term behavior of LRNNs is related to that of ESNs. For the latter, usually the activation function is \tanh and the spectral radius is smaller than 1. Then reservoirs collapse because of $|\tanh(z)| \leq |z|$ for all $z \in \mathbb{R}$, but the convergence may be rather slow. Nonetheless it guarantees contractivity and hence for any fixed input (not just the origin) the system converges to a unique fixed point. This leads to the so-called *echo state property* [48]: Any random initial state of a reservoir is forgotten such that, after a washout period, the current network state is a

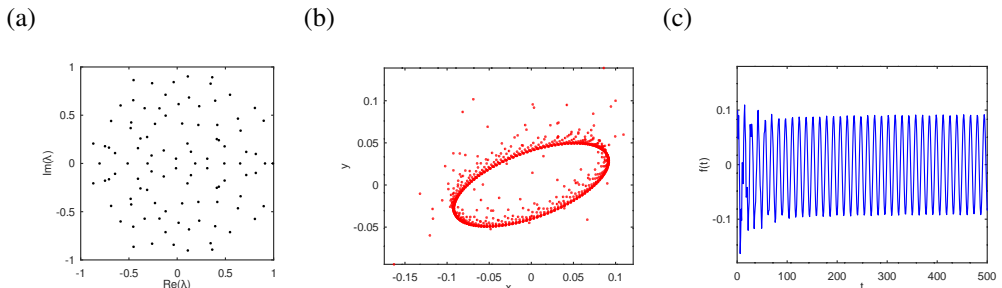


Figure 3 Dynamic system behavior of a pure random reservoir with unit spectral radius, with $N^{\text{res}} = 100$ neurons: (a) Eigenvalue spectrum of the reservoir matrix W^{res} with complex conjugate eigenvalue pairs in the complex plane. (b) Visualization of $f(t)$ by planar projection. In the long run, we get an ellipse trajectory, thus only two dimensions (cf. Equation 8). (c) Projected to one (arbitrary) dimension, we have pure sinusoids with one single angular frequency for large t , sampled in large steps.

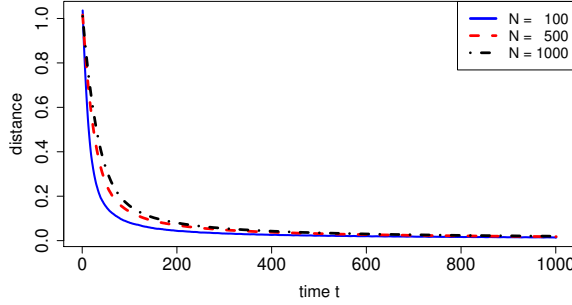


Figure 4 Asymptotic behavior of pure random reservoirs with unit spectral radius: The (Euclidean) distance between the actual value $f(t)$ (according to Equation 7) and its approximation by the final ellipse trajectory (Equation 8) is almost zero already after a few hundred steps. The figure shows the distances for $N^{\text{res}} = 100$ (solid/blue), $N^{\text{res}} = 500$ (dashed/red), and $N^{\text{res}} = 1000$ (dotted/black) random reservoir neurons, starting with a random vector of unit length, averaged over 1000 trials.

function of the driving input. In contrast to ESNs, LRNNs have linear activation and a spectral radius of exactly 1 (cf. Definition 3). But as we have just shown, there is a similar effect in the long run: The network activity reduces to at most two dimensions – independent of the initial state of the network.

4 Learning LRNNs

Functions can be learned and approximated by LRNNs in two steps: First, as for ESNs [11], we only learn the output weights W^{out} (cf. Section 4.1). The input weights W^{in} and reservoir weights W^{res} are arbitrary random values and remain unchanged (cf. Definition 3). Nevertheless, in order to obtain better numerical stability during the computation, they are adjusted as follows:

- Because of the linear activation, the spectral radius of the reservoir weights matrix W^{res} is set to 1 (cf. Definition 3). Otherwise, with increasing t , the values of $f(t) = W^t \cdot s$ explode if the spectral radius is greater or vanish if the spectral radius is smaller than 1 (cf. Section 3.4). In consequence, the overall learning procedure behaves rather stable.
- Furthermore, we initialize the reservoir neurons such that the reservoir start vector r (with N^{res} components) has unit norm by setting:

$$r = \frac{1}{\sqrt{N^{\text{res}}}} \cdot [1 \cdots 1]^{\top}$$

It is part of the (overall) start vector $s = \begin{bmatrix} S(0) \\ r \end{bmatrix}$ (cf. Section 3).

- We employ fully connected graphs, i.e., all, especially the reservoir neurons are connected with each other, because the connectivity has nearly no influence on the best reachable performance [49].

Second, if possible, we reduce the network size (cf. Section 4.3). This often leads to better generalization and avoids overfitting. Thus, in contrast to many other approaches, the network architecture is changed during the learning process, and we do not do this by incremental derivation from the original network but in only one step.

4.1 Learning the Output Weights

To learn the output weights W^{out} , we run the input values from the time series $S(0), \dots, S(n)$ through the network (in input receiving mode), particularly through the reservoir. This means, we build the sequence of corresponding reservoir states $R(0), \dots, R(n)$ where the reservoir start vector r (see above) in principle can be chosen arbitrarily but with all nonzero entries (cf.

Property 4):

$$R(t_0) = r \text{ and } R(t + \tau) = [W^{\text{in}} \ W^{\text{res}}] \cdot \begin{bmatrix} S(t) \\ R(t) \end{bmatrix} = W^{\text{in}} \cdot S(t) + W^{\text{res}} \cdot R(t) \quad (9)$$

We want to predict the next input value $S(t + \tau)$, given the current input and reservoir states $S(t)$ and $R(t)$. To achieve this, we comprise all but the last input and reservoir states in one matrix X with:

$$X = \begin{bmatrix} S(0) & \cdots & S(n-1) \\ R(0) & \cdots & R(n-1) \end{bmatrix} \quad (10)$$

Each output value shall correspond to the respective next input value $S(t + \tau)$. Therefore, we compose another matrix

$$Y^{\text{out}} = [S(1) \cdots S(n)] \quad (11)$$

consisting of the next values of the time series S to be predicted where the first value $S(0)$ clearly has to be omitted because it has no predecessor value. We compute $Y^{\text{out}}(t) = S(t + \tau)$ from $X(t)$ by assuming a linear dependency:

$$Y^{\text{out}} = W^{\text{out}} \cdot X \quad (12)$$

Its solution can easily be determined as $W^{\text{out}} = Y^{\text{out}}/X$, where $/$ denotes right matrix division, i.e., the operation of solving a linear equation system, possibly applying the least squares method in case of an overdetermined system, as implemented in many scientific programming languages such as Matlab [50] or Octave [51]. Prediction of further values is now possible (in output generating mode) as follows:

$$\begin{bmatrix} S(t + \tau) \\ R(t + \tau) \end{bmatrix} = W \cdot \begin{bmatrix} S(t) \\ R(t) \end{bmatrix} \text{ with } W \text{ as in Equation 1} \quad (13)$$

Property 7 (treatment of multiple sequences). It is also possible to learn from multiple sequences at once. For this, let several time series S_1, \dots, S_K in d dimensions with (not necessarily identical) lengths n_1, \dots, n_K be given. For each S_k with $1 \leq k \leq K$, we determine:

- the sequence of corresponding reservoir states R_k (according to Equation 9), taking always the same reservoir start vector r ,
- the corresponding input matrix X_k (according to Equation 10), and
- the corresponding predicted output matrix Y_k^{out} (according to Equation 11).

We aggregate the input and output matrices to $X = [X_1 \cdots X_K]$ and $Y^{\text{out}} = [Y_1^{\text{out}} \cdots Y_K^{\text{out}}]$ with $n_1 + \cdots + n_K$ columns each. Solving the linear matrix equation $Y^{\text{out}} = W^{\text{out}} \cdot X$ (identical with Equation 12) finally yields the output weight matrix W^{out} .

This first phase of the learning procedure is related to a linear *autoregressive model* [35]. However, one important difference to an autoregressive model is that for LRNNs the output does not only depend on its own previous values and possibly white noise but on the complete state of the possibly big reservoir whose dynamics is explicitly dealt with in the reservoir matrix W^{res} . The reservoir effectively allows us to do arbitrary auxiliary computation such that any (nonlinear) function $f(t)$ can be approximated by an LRNN (cf. Property 8).

4.2 An Approximation Theorem

Property 8. From a function $f(t)$ in $d \geq 1$ dimensions, let a series of function values $f(t_0), \dots, f(t_n)$ be given. Then there is an LRNN with the following properties:

1. It runs exactly through all given $n + 1$ function values, i.e., it approximates $f(t)$.
2. It can effectively be learned by the LRNN learning procedure (Section 4.1) employing

$$N^{\text{res}} \geq n - N^{\text{inout}} \quad (14)$$

reservoir neurons.

Proof. See Section E. □

Therefore, at least in theory, any time-dependent function $f(t)$ can be interpolated, i.e., exactly approximated on the given function values and continued on input other than nonnegative integer numbers (cf. Remark 1), although clearly not every function can be implemented by LRNNs, in particular functions increasing faster than single-exponential (cf. Property 5) such as 2^t (double-exponential) or $t!$ (factorial function). Also in practice, the LRNN learning procedure performs rather well (cf. Section 5).

Nevertheless, the matrix X may be ill-conditioned for long input sequences, because the reservoir state sequence as part of the matrix X reduces to at most two dimensions for large t , independent of the number of reservoir neurons (cf. Section 3.4). Hence, the rank of the matrix X may not be maximal and consequently Equation 12 may not be solvable numerically in practice (although we may have an equation system with the same number of equations and unknowns). A simple increase of the number of reservoir neurons does not help much.

However, one could learn not only the output weights W^{out} as in ESNs but the complete transition matrix W : For this, we employ a random reservoir state sequence matrix $[R(0) \cdots R(n)]$ with N^{res} reservoir neurons, considered as additional input. If all elements of this matrix are random numbers, independently and identically distributed from the standard normal distribution, its rank is almost always maximal, because the original and the additional (random) inputs are throughout linearly independent of each other. This procedure therefore avoids the ill-conditioning of the matrix X . We then just have to solve the linear matrix equation $Y = W \cdot X$ (cf. Equation 12) with

$$Y = \begin{bmatrix} S(1) & \cdots & S(n) \\ R(1) & \cdots & R(n) \end{bmatrix}$$

and X as in Equation 10. By this, the input and reservoir weights W^{in} and W^{res} are learned, not only the output weights W^{out} . But our experiments indicate that this procedure is less reliable than the one with given, i.e., predefined random input and reservoir weights and unit spectral radius for the reservoir (cf. Section 4.1), at least if the whole (and not only a part of) the reservoir is learned from additional (random) input.

The topic of learning all weights in the matrix W is investigated in [52] for ESNs with nonlinear activation function in the reservoir. However, for LRNNs, the given input and reservoir weights W^{in} and W^{res} together with the learned output weights W^{out} already provide the best approximation of the function $f(t)$. There is no need to learn the input and reservoir weights, simply because LRNNs are completely linearly activated RNNs (including the reservoir). If one tries to learn W^{in} and W^{res} taking not only the output time series S but additionally the reservoir state time series R into account, then exactly the given input and reservoir weights are learned if Equation 14 holds. Only with nonlinear activation there is a learning effect.

Although LRNNs rely on linear activation functions, they can represent nonlinear functions $f(t)$. In fact, LRNNs are well suited to represent differential equations (cf. Property 1), which lead to highly nonlinear functions. Any exponential, trigonometric and polynomial functions can be modeled (cf. Property 2). There is no restriction to cyclic or periodic time series. Any time-dependent function $f(t)$ can be exactly approximated (cf. Property 8), including functions with regime shifts. This is also true for chaotic functions such as random number series or the Mackey-Glass time series [53, 11]. However, long-term prediction is not that accurate for these types of time series.

Remark 2 (scope and generalization to nonlinear activation). This paper focuses on time-dependent functions $f(t)$, where the output evolves autonomously over time. Such functions are central to modeling dynamic systems and are naturally handled by LRNNs with purely linear activation. In this setting, nonlinearities are not required: The network dynamics, governed by the transition matrix, already permit the approximation of a broad class of functions, including polynomials, exponentials, and oscillatory signals (cf. Property 8).

A different problem is to compute general functions $f(s)$, i.e., mappings from arbitrary input vectors s to output values. In that context, nonlinear activation functions may offer benefits. If the activation function g is monotonic and invertible, the LRNN learning procedure introduced so far (Section 4.1) can, in principle, be extended. For this, g has to be applied component-wise to Equation 9 while running the input through the reservoir and to Equation 12. The solution of the resulting equation $Y^{\text{out}} = g(W^{\text{out}} \cdot X)$ is then just $W^{\text{out}} = g^{-1}(Y^{\text{out}})/X$.

However, the network size reduction procedure introduced next (Section 4.3) relies on linear activation and is therefore not applicable when nonlinear activation is used. In such cases, approximation may still be possible, but the reduction method would no longer preserve precision because (the proof of) Property 4 requires the commutativity of matrix multiplication with Jordan matrices J , which does not hold any longer if nonlinear activation is employed.

Property 8 is related to the *universal approximation theorem* for feedforward neural networks [54]. It states that a (non-recurrent) network with a linear output layer and at least one hidden layer activated by a nonlinear, sigmoidal function can approximate any continuous function on a closed and bounded subset of the \mathbb{R}^n from one finite-dimensional space to another with any desired nonzero amount of error, provided that the network is given enough hidden neurons [2, Section 6.4.1]. Since RNNs are more general than feedforward networks, the universal approximation theorem also holds for them [55]. Any measurable function can be approximated with a (general) recurrent network arbitrarily well in probability [56].

Remark 3. Any time series $S(0), \dots, S(n)$ can be generated by employing a backward shift matrix, i.e., a binary matrix with 1s on the subdiagonal and 0s elsewhere [46, Section 0.9.7], as transition matrix W and $s = [S(0) \cdots S(n)]^\top$ as start vector. But such a network clearly would have no ability to generalize to future data. Fortunately, this does not hold for a transition matrix W learned by the procedure in Section 4.1. Furthermore, the eigenvalue spectrum of the backward shift matrix is empty, whereas that of the learned W is not, which is important for network size reduction introduced in Section 4.3.

4.3 Network Size Reduction

To approximate a function exactly for sure, we need a large number N^{res} of reservoir neurons (cf. Property 8 and Equation 14). It is certainly a good idea to lower this number. One could do this by simply taking a smaller number of reservoir neurons, but then a good approximation cannot be guaranteed. In what follows, we therefore reduce the dimensionality of the transition matrix W in a more controlled way – after learning the output weights. Our procedure of dimensionality reduction leads to smaller networks with sparse connectivity. In contrast to other approaches, we do not learn the new network architecture by incremental derivation from the original network, e.g., by removing unimportant neurons or weights, but in one step by inspecting the eigenvalues of the transition matrix.

For ESNs, dimensionality reduction is considered, too, namely by means of so-called *conceptors* [13, 14, 57]. These are special matrices which restrict the reservoir dynamics to a linear subspace that is characteristic for a specific pattern. However, as in principal component analysis (PCA) [58], conceptors reduce only the spatial dimensionality of the point cloud of the given data. In contrast to this, for LRNNs, we reduce the transition matrix W and hence take also into account the temporal order of the data points in the time series. By applying insights from linear algebra, the actual network size can be reduced and not only the subspace of computation as with conceptors.

Property 9. By Property 4, the function $f(t) = W^t \cdot s$ can be rewritten by means of the Jordan matrix of the transition matrix W as $A \cdot J^t \cdot y$, where the start vector can be chosen as nonzero constant, e.g., $y = [1 \cdots 1]^\top$. Furthermore, by Property 2, $f(t)$ can be expressed as a sum of vectors $u = v \cdot J_m(\lambda)^t \cdot w$ where w is constant because it is part of the start vector y . Then it follows from Property 6 that for large t the contribution of a Jordan component vanishes if $\|v\| \approx 0$ and/or $|\lambda| \ll 1$.

In consequence, we omit all Jordan components causing only small errors, until a given threshold is exceeded. The error E of a network can be estimated by the root-mean-square error

(RMSE) normalized to the number of all sample components between input x and predicted output y :

$$\text{RMSE}(x, y) = \sqrt{\frac{1}{n} \sum_{t=1}^n \|x(t) - y(t)\|^2}$$

We shall omit all network components corresponding to Jordan blocks $J_m(\lambda)$ with smallest errors as long as the RMSE is below a given threshold θ . Network components that are not omitted are considered *relevant*. Thus, from A , J , and y (according to Property 4), we successively derive reduced matrices A and J and the vector y as follows:

- Reduce A to the rows corresponding to the input/output components and the columns corresponding to the relevant network components.
- Reduce J to the rows and columns corresponding to the relevant network components.
- Reduce y to the rows corresponding to the relevant network components.

Note that the dimensionality reduction does not only lead to a smaller number of reservoir neurons but also to a rather simple network structure: The transition matrix J (which comprises the reservoir weights W^{res} of the reduced network) is a sparse matrix with nonzero elements only on the main and immediately adjacent diagonals. Thus, the number of connections is in $O(N)$, i.e., linear in the number of reservoir neurons, not quadratic – as in general.

Figure 5 summarizes the overall learning procedure for LRNNs including network size reduction. It has been implemented by the authors in Octave. Note that, although the Jordan matrix J (cf. Property 2) may contain eigenvalues with multiplicity greater than 1, Octave does not always calculate exactly identical eigenvalues then. Therefore, we cluster the computed eigenvalues as follows: If the distance in the complex plane between eigenvalues is below some given small threshold δ , they are put into the same cluster which eventually is identified with its centroid. Thus it is a kind of single linkage clustering [59]. In our approach, the Jordan components are considered in decreasing order of their relevance, sorted by the RMSE that their omission causes. Therefore, they cannot be removed by mistake, provided that a reasonable threshold θ is taken. However, in our network size reduction procedure (which is not a simple pruning), we use a binary search (cf. Figure 5). It handles a large group of similarly relevant eigenvalues in one step. This speeds up the procedure considerably, although it is a kind of approximation. The complete implementation of the learning procedure together with some case studies (cf. Section 5) is publicly available at <http://github.com/OliverObst/decorating/>.

Example 4. Let us illustrate the LRNN learning procedure (Figure 5) with the Fibonacci series (Example 2). We start with the first values of the Fibonacci series $f(0), \dots, f(n)$ as input S (lines 1-3) and generate a random reservoir of size N^{res} (lines 4-6). After learning the output weights W^{out} (lines 7-10) and decomposing the resulting transition matrix W (lines 11-15), the network size reduction procedure (lines 16-24) often yields minimal networks with only two reservoir neurons representing

$$f(t) \stackrel{\text{Property 4}}{=} A \cdot J^t \cdot y \text{ with } A \approx \begin{bmatrix} \frac{1}{\sqrt{5}} & -\frac{1}{\sqrt{5}} \end{bmatrix} \text{ and } J \approx \begin{bmatrix} \lambda_1 & 0 \\ 0 & \lambda_2 \end{bmatrix} \text{ for } y = \begin{bmatrix} 1 \\ 1 \end{bmatrix}$$

where the eigenvalues λ_1 and λ_2 are as in Binet's formula (Equation 3). For instance, for $N^{\text{res}} = n = 30$ and precision threshold $\theta = 0.001$, we obtain minimal networks in 32% of the cases from 100 trials. They belong to the best networks with respect to their RSME. Thus, by employing a standard validation procedure, the LRNN in Figure 2(c) actually can be derived numerically by the LRNN learning procedure with network size reduction.

Note that the spectral radius of the reservoir weights matrix W^{res} remains 1 all the time (cf. Definition 3). However, after learning the output weights W^{out} , the spectral radius of the overall transition matrix W (according to Equation 1) and hence of the matrix J may be greater than 1 if the function $f(t)$ to be modeled is exponentially increasing. This obviously holds for the Fibonacci series (because of $\lambda_1 > 1$).

- 1: % d -dimensional function f , given sampled, as time series S , and start vector s
- 2: $S = [f(0) \cdots f(n)]$
- 3: $s = \begin{bmatrix} S(0) \\ r \end{bmatrix}$ where $r = \frac{1}{\sqrt{N^{\text{res}}}} \cdot \left[\underbrace{1 \cdots 1}_{N^{\text{res}} \text{ times}} \right]^{\top}$
- 4: % random initialization of input and reservoir weights
- 5: $W^{\text{in}} = \text{randn}(N^{\text{res}}, d)$
- 6: $W^{\text{res}} = \text{randn}(N^{\text{res}}, N^{\text{res}})$ normalized to unit spectral radius
- 7: % learn output weights by linear regression
- 8: $X = [W^t \cdot s]_{t=0, \dots, n}$ % run in input receiving mode
- 9: $Y^{\text{out}} = [S(1) \cdots S(n)]$
- 10: $W^{\text{out}} = Y^{\text{out}} / X$
- 11: % transition matrix and its decomposition
- 12: $W = \begin{bmatrix} W^{\text{out}} \\ W^{\text{in}} \quad W^{\text{res}} \end{bmatrix}$
- 13: $J = \text{jordan_matrix}(W)$ with components k sorted in decreasing order
- 14: with respect to $\text{Error}(J_{\langle 1, \dots, k-1, k+1, \dots, K \rangle})$
- 15: where $K = \# \text{Jordan components in } J$
- 16: % network size reduction (with binary search)
- 17: $L = 1$ % left index border
- 18: $R = K$ % right index border
- 19: while $(L \neq R)$
- 20: $M = \left\lfloor \frac{L+R}{2} \right\rfloor$
- 21: if $\text{Error}(J_{\langle 1, \dots, M \rangle}) < \theta$
- 22: then $R = M$
- 23: else $L = M + 1$
- 24: return(M)
- 25: % subroutine $\text{Error}(J_I)$
- 26: % compute error for Jordan matrix reduced to indexed components
- 27: reduce J to components indexed by I
- 28: $y = [1 \cdots 1]^{\top}$
- 29: $Y = [J^t \cdot y]_{t=0, \dots, n}$ % run in output generating mode
- 30: $A = X / Y$ with rows restricted to input/output dimensions
- 31: return($\text{RMSE}(S, A \cdot Y)$)

Figure 5 Pseudocode for learning LRNNs including network size reduction. A binary search algorithm is employed for determining the relevant network components with smallest errors. For this, the network components are sorted by their RMSE. The program returns the number M of relevant components in the Jordan matrix J (line 24). The subroutine $\text{Error}(J)$ (lines 25-31) computes the error of the predicted output for the Jordan matrix reduced to the components indexed by I .

4.4 Complexity and Generalization of the Procedure

Remark 4. In both learning steps, it is possible to employ any of the many available fast and constructive algorithms for linear regression and eigendecomposition [60]. Therefore, the time complexity is just $O(N^3)$ for both output weights learning and network size reduction. In theory, if we assume that the basic numerical operations such as $+$ and \cdot can be done in constant time, the asymptotic complexity is even a bit better. In practice, however, the complexity depends on the bit length of numbers in floating point arithmetic, of course, and may be worse hence. The size of the learned network is in $O(N)$ (cf. Section 4.3).

Note that, in contrast, feedforward networks with three threshold neurons already are NP-hard to train [61]. This results from the fact that the universal approximation theorem

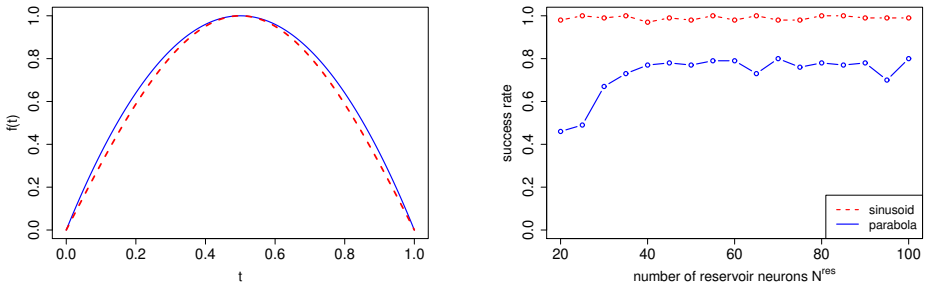


Figure 6 **Left:** Graphs for Example 5: a parabola and a sinusoid. The question is: which one is which? Both can be learned and distinguished by LRNNs from the visually similar positive parts of the respective graphs, i.e., function values for $t \in [0, 1]$. In this interval, all values of the parabola (solid/blue) are greater than or equal to those of the sinusoid (dashed/red). **Right:** For Example 5, how often LRNNs of minimal size are learned after network size reduction, i.e., with $N_1 = 3$ neurons for the parabola and $N_2 = 2$ neurons for the sinusoid? The diagram shows the success rate of the learning procedure in this regard as a function of the number of reservoir neurons N^{res} before network size reduction (for 100 trials). Networks of minimal size are learned starting already with $N^{\text{res}} = 40$ reservoir neurons in about 77% (parabola, solid/blue) or 99% (sinusoid, dashed/red) of the trials.

for feedforward networks differs from Property 8 because the former holds for multivariate functions and not only time-dependent input. In this light, the computational complexity of $O(N^3)$ for LRNNs does not look overly expensive. It dominates the overall time complexity of the whole learning procedure because it is not embedded in a time-consuming iterative learning procedure (such as backpropagation) as in other state-of-the-art methods.

Remark 5. We observe that most of the results presented in this paper still hold if the transition matrix W contains complex numbers. This means in particular that also complex functions can be learned (from complex-valued time series) and represented by LRNNs (Property 8). Nonetheless, the long-term behavior of networks with a random complex transition matrix W differs from the one described in Section 3.4 because then there are no longer pairs of complex conjugate eigenvalues.

5 Experiments

In this section, we demonstrate evaluation results for learning and predicting time series, approximating them by a function $f(t)$ represented by an LRNN, for several tasks. We consider the following benchmarks: multiple superimposed oscillators (MSO), number puzzles, robot soccer simulation, and predicting stock prices. All experiments are performed with a program written by the authors in Octave [51] (cf. Section 4.3). There is also a reimplementation in Python available (see <http://github.com/OliverObst/lrnn>). Let us start with an example that illustrates the overall method.

Example 5. The graphs of the functions $f_1(t) = 4t(1-t)$ (parabola) and $f_2(t) = \sin(\pi t)$ (sinusoid) look rather similar for $t \in [0, 1]$ (cf. Figure 6 Left). Can both functions be learned and distinguished from each other by our LRNN learning procedure (cf. Section 4)?

To investigate this, we sample both graphs for $t \in [0, 1]$ with time step $\tau = 0.01$. After that, we learn the output weights W^{out} (cf. Section 4.1), starting with a large enough reservoir consisting of up to $N^{\text{res}} = 100$ neurons (cf. Property 8). Finally, we reduce the size of the overall transition matrix W with precision threshold $\theta = 0.01$ and cluster threshold $\delta = 0.03$ (cf. Section 4.3). Minimal LRNNs consist of $N_1 = 3$ neurons for the parabola (cf. Example 1) and $N_2 = 2$ neurons for the sinusoid (cf. Section 3.4). The networks of minimal size are learned already with $N^{\text{res}} = 40$ reservoir neurons before network size reduction in about 77% (parabola) or 99% (sinusoid) of the trials (cf. Figure 6 Right). Learning the parabola is more difficult because the corresponding transition matrix W (cf. Example 1) has no proper eigendecomposition according to Property 3 but only a Jordan decomposition according to Property 2.

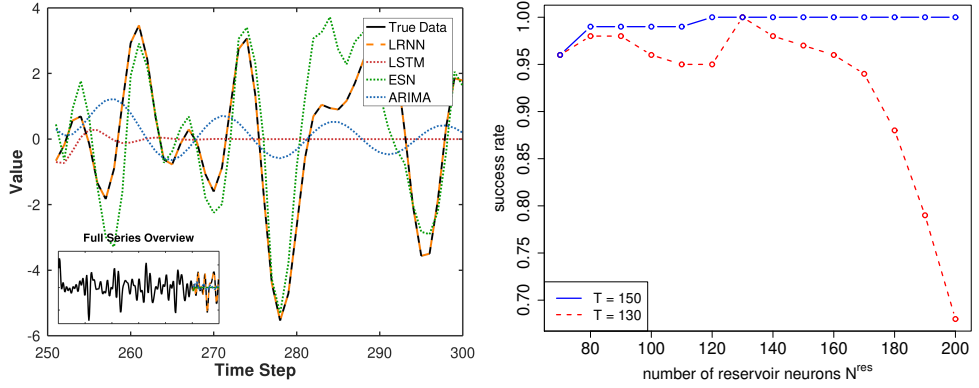


Figure 7 **Left:** The signal $S(t)$ of $K = 8$ multiple superimposed oscillators (for $1 \leq t \leq 300$ and time step $\tau = 1$) does not have a simple periodic structure (small figure). LRNN learning leads to minimal networks with only $N = 16 = 2K$ reservoir neurons, i.e., two for each frequency in the signal, with RMSE less than 10^{-5} (dashed line). Other methods do not perform so well on the MSO benchmark (cf. dotted lines). **Right:** Experimental results for the MSO benchmark ($K = 8$). The diagram shows the success rate (from 100 trials): From an initial reservoir size of N^{res} neurons, how often is the minimal LRNN with size $N = 16$ learned? The two curves are for different lengths T of the time series $S(t)$ used for training. Already for $T = 150$ (solid/blue), a minimal-size LRNN is learned in at least 96% of the trials if $N^{\text{res}} \geq 70$. For these minimal LRNNs, the RMSE is smaller than 10^{-5} . As one can see, for $T = 130$ (dashed/red) the given information does not always suffice and leads to overfitting.

5.1 Multiple Superimposed Oscillators

Example 6. Multiple superimposed oscillators (MSO) count as difficult benchmark problems for RNNs [49, 62]. The corresponding time series is generated by summing up several (pure) sinusoids. Formally it is described by

$$S(t) = \sum_{k=1}^K \sin(\alpha_k t)$$

where $K \leq 8$ denotes the number of sinusoids and $\alpha_k \in \{0.200, 0.311, 0.420, 0.510, 0.630, 0.740, 0.850, 0.970\}$ their frequencies.

Various publications have investigated the above MSO problem with different numbers of sinusoids. We concentrate here solely on the most complex case $K = 8$ because in contrast to other approaches it is still easy to learn for LRNNs. Applying the LRNN learning procedure with precision threshold $\theta = 0.5$, we arrive at LRNNs with only $N = 16$ reservoir neurons and an RMSE less than 10^{-5} (cf. Figure 7 Left). If we start with a large enough reservoir (cf. Figure 7 Right). Since two neurons are required for each frequency (cf. Section 3.4), $2K = 16$ is the minimal reservoir size. Thus LRNNs outperform the previous state-of-the-art for the MSO task with a minimal number of units. Previous results [49] report $N^{\text{res}} = 68$ as the optimal reservoir size for ESNs, but in contrast to our approach, this number is not further reduced.

For a more systematic evaluation, we generalize the MSO benchmark (Example 6) by considering 20 times $K = 8$ random frequencies $\alpha_1, \dots, \alpha_8$ uniformly distributed on the interval $[0, 1]$. We take the first 250 time steps, i.e., $t = 1, \dots, 250$, as training data and the subsequent 50 time steps as testing data and compare the performance of LRNNs with other approaches (cf. Section 2) with respect to their RSME on the testing data, partially using the Python library Darts [63, see also <http://unit8co.github.io/darts/>] for time series, including (a) a simple baseline, namely predicting constantly the arithmetic mean of the training data, (b) ARIMA using the AutoARIMA package [37], (c) the simple sparse ESN demo by Mantas Lukoševičius from http://mantas.info/code/simple_esn/ employing ReservoirPy [64], (d) an LSTM forecasting model implemented in Darts with hyperparameter optimization, and (e) LRNNs where we adopt validation data as above and choose the best model with respect to the RMSE on the validation data from 100 trials.

Table 1 shows the evaluation results. As one can see, LRNNs outperform all other approaches on this benchmark by far. The reason for this is certainly the network size reduction

procedure (cf. Section 4.3), unique in our approach, because it exactly selects the relevant components of the network: Each complex conjugate eigenvalue pair corresponds to one of the frequencies $\alpha_1, \dots, \alpha_8$. In general, an LRNN with $2K$ neurons suffices to represent a signal, which might be a musical harmony [65], consisting of K sinusoids (cf. Section 3.4). It can be learned by the LRNN learning procedure with network size reduction. However, if several frequencies are close to each other (cf. Example #1 in Table 1) or are rather small (cf. Example #12), then LRNNs do not perform quite so well.

LRNNs are also advantageous considering the time required to train a well performing model with less than 3 s per series for training and testing on average:

	Arima (R)	Arima (Python)	ESN	LSTM	LRNN
train + test time	0.35 s	3.20 s	1.24 s	125.43 s	2.97 s

The ARIMA experiments with an R implementation are fastest (0.35 s per series) but often perform even worse than our baseline. Interestingly, an ARIMA implementation in Python turns out to be significantly slower (3.20 s per series). ESN learning takes 1.24 s per series. LRNNs more or less extend the ESN approach and take 2.97 s per series on average with our approach, including required repeated reservoir generations. LSTM learning including hyperparameter selection takes 125.4 s per series. All experiments are run on an Intel i9-10940X, 3.3 GHz CPU, and 128 GB RAM.

5.2 Solving Number Puzzles

Example 7. Number series tests are a popular type of intelligence test. The function represented by a number series can often be learned also by artificial neural networks, in particular RNNs. In [5], 20 number puzzles are listed [cf. 4]. Among them are the series:

$$\begin{aligned} S_8 &= [28, 33, 31, 36, 34, 39, 37, 42] \quad f(t) = f(t-2) + 3 \\ S_9 &= [3, 6, 12, 24, 48, 96, 192, 384] \quad f(t) = 2f(t-1) \\ S_{15} &= [6, 9, 18, 21, 42, 45, 90, 93] \quad f(t) = 2f(t-2) + 4.5 + 1.5(-1)^{t-1} \\ S_{19} &= [8, 12, 16, 20, 24, 28, 32, 36] \quad f(t) = f(t-1) + 4 \end{aligned}$$

We apply the LRNN learning procedure to all 20 number puzzles taking small reservoirs because the number series are short. As a side effect, this leads to learning more general functions, which seems to be fully adequate because number puzzles are usually presented to humans. The first 7 of 8 elements of each series are given as input. In each trial, we repeatedly generate LRNNs, until the RMSE is smaller than $\theta = 0.1$. Then the last (8th) element of the respective series is predicted (according to Equation 13) and rounded to the nearest integer because all considered number series are integer.

Table 2 lists the percentages of correct predictions of the last element for different settings. Here, the series with definitions recurring to $f(t-2)$ but not $f(t-1)$, e.g., S_8 and S_{15} , turned out to be the most difficult. If we add the previous values of the time series, i.e., $f(t-2)$, as clue to the input, then the correctness of the procedure increases significantly: For 19 of 20 number puzzles, the most frequently predicted last element (simple majority) is the correct one. It is predicted in 76.5% on average over all trials and number puzzles. Let us remark that the whole evaluation with altogether $20 \cdot 50 \cdot 1000 = 1000000$ trials including possibly repeated network generation ran in only a few minutes on standard hardware.

Although the application domains of transformer models [66] and LRNNs are different, one can compare modern LLMs and LRNNs with respect to solving number puzzles: LLMs can yield interpretable explanations. For example, ChatGPT (which is based on GPT-4, cf. Section 2.3) correctly predicts the next value for all number puzzles, but in 2 of 20 cases finds incorrect (recursive or closed) formulae explaining the number puzzles (cf. Section F). The LRNN learning procedure with network size reduction determines LRNNs with small reservoir sizes. From these, we can read off explicit, i.e., also interpretable, small formulae for the number series, e.g., $f(t) = 3 \cdot 2^n$ for S_9 with a minimal reservoir size $N^{\text{res}} = 1$. Focusing on small reservoir sizes (determined from 1000 trials), for 18 of 20 number puzzles, the most

#	frequencies	α_1	α_2	α_3	α_4	α_5	α_6	α_7	α_8	Baseline	ARIMA	ESN	LSTM	units	RMSE	units	RMSE	units	RMSE	LRNN
1	0.334	0.336	0.399	0.403	0.412	0.438	0.442	0.724	2.05613	2.07496	0.23208	5 + 32	0.16038	10	0.04761					
2	0.049	0.091	0.161	0.292	0.472	0.715	0.832	0.997	2.25490	3.06428	0.19716	10 + 2	0.19218	16	0.00051					
3	0.308	0.521	0.597	0.607	0.736	0.766	0.924	0.957	1.34810	1.46533	0.13680	5 + 8	0.11722	16	0.00060					
4	0.031	0.348	0.448	0.476	0.613	0.628	0.833	2.03748	2.13161	0.25979	5 + 8	0.19209	14	0.0003						
5	0.059	0.239	0.324	0.421	0.437	0.519	0.747	0.777	1.68045	2.41015	0.16561	10 + 1	0.14548	16	0.00011					
6	0.013	0.029	0.262	0.543	0.636	0.705	0.740	0.807	1.79038	2.91774	0.19343	5 + 4	0.16770	16	0.00038					
7	0.155	0.226	0.286	0.512	0.661	0.692	0.746	0.930	1.48729	1.75658	0.13109	5 + 4	0.13761	16	0.00012					
8	0.017	0.027	0.273	0.475	0.616	0.848	0.962	0.989	1.87712	2.66991	0.22200	5 + 2	0.16481	16	0.02033					
9	0.092	0.318	0.335	0.413	0.593	0.743	0.747	0.799	1.84272	2.31084	0.22680	5 + 64	0.16025	16	0.00142					
10	0.108	0.122	0.262	0.307	0.391	0.577	0.589	0.603	1.64237	1.66822	0.18361	10 + 16	0.13289	16	0.00772					
11	0.071	0.264	0.557	0.609	0.641	0.719	0.853	0.964	1.71070	2.01792	0.13613	5 + 16	0.14964	16	0.00003					
12	0.036	0.052	0.062	0.222	0.279	0.316	0.563	0.672	1.52224	1.83523	0.18562	10 + 8	0.15571	14	0.15984					
13	0.036	0.481	0.571	0.724	0.750	0.750	0.864	0.898	2.51888	2.50217	0.15961	5 + 16	0.2408	14	0.00067					
14	0.175	0.220	0.258	0.419	0.487	0.513	0.628	0.663	2.17787	1.90370	0.23698	5 + 8	0.19731	16	0.00069					
15	0.185	0.300	0.461	0.751	0.814	0.833	0.840	0.992	2.18527	1.63141	0.15527	5 + 2	0.20639	14	0.03709					
16	0.088	0.120	0.137	0.245	0.478	0.793	0.797	0.992	2.27108	2.51581	0.15872	10 + 1	0.19325	16	0.01439					
17	0.002	0.242	0.348	0.503	0.734	0.748	0.759	0.862	1.47542	1.76223	0.23496	10 + 8	0.13808	16	0.00150					
18	0.018	0.352	0.583	0.625	0.714	0.824	0.838	0.888	2.44582	2.71492	0.24585	5 + 32	0.25433	16	0.00010					
19	0.046	0.105	0.263	0.351	0.517	0.556	0.758	0.807	1.79806	2.24052	0.18220	5 + 16	0.18124	16	0.00005					
20	0.091	0.141	0.375	0.578	0.686	0.785	0.951	0.996	2.05839	2.21768	0.15490	5 + 32	0.17551	16	0.00001					

Table 1 Evaluation results for 20 generalized MSO examples with 8 randomly generated frequencies each. The best performing approach is highlighted by bold face. For the LSTMs, the number of input and hidden units of the best performing neural network is given. For LRNNs, the network size N after network size reduction is shown.

frequently predicted last element is the correct one. Hence, network size reduction can improve the generalization and explanation ability of LRNNs because it may suppress noise. However, for complex applications with high variability and noise, the network size reduction procedure clearly does not lead to such a strong compression of the network (cf. Section 5.3).

series	$N^{\text{res}} = 3$	$N^{\text{res}} = 4$	$N^{\text{res}} = 5$	with reduction	$\min(N^{\text{res}})$	plus clue
S_1	2.2%	1.3%	1.3%	64.4%	3	33.4%
S_2	37.6%	42.2%	29.4%	100.0%	2	100.0%
S_3	5.4%	4.1%	1.1%	99.5%	2	100.0%
S_4	23.8%	24.2%	16.8%	81.5%	2	99.9%
S_5	56.9%	57.6%	44.2%	99.1%	2	99.7%
S_6	31.7%	33.7%	16.1%	56.6%	2	100.0%
S_7	72.8%	68.2%	56.2%	99.2%	2	100.0%
S_8	5.1%	3.4%	1.3%	86.0%	3	76.3%
S_9	100.0%	100.0%	100.0%	100.0%	1	100.0%
S_{10}	48.9%	71.5%	67.6%	83.3%	2	100.0%
S_{11}	10.6%	9.0%	3.4%	96.9%	2	100.0%
S_{12}	23.8%	21.1%	11.0%	82.4%	2	43.2%
S_{13}	56.5%	58.1%	41.5%	95.1%	2	99.8%
S_{14}	6.7%	7.4%	2.1%	94.3%	2	87.1%
S_{15}	1.6%	2.6%	2.5%	3.6%	4	1.1%
S_{16}	6.8%	5.9%	3.4%	88.7%	3	73.3%
S_{17}	11.9%	12.0%	6.8%	51.6%	3	41.0%
S_{18}	3.1%	2.0%	1.1%	37.5%	4	18.0%
S_{19}	59.6%	70.1%	72.0%	99.0%	2	99.8%
S_{20}	1.5%	0.5%	0.6%	57.9%	4	57.2%

Table 2 Percentages of correct predictions of the last element for 20 number puzzles [4, 5] in 1000 trials for different settings: (a) with fixed reservoir size $N^{\text{res}} = 3, 4, 5$; (b) with network size reduction starting with $N^{\text{res}} = 7$ reservoir neurons yielding small/minimal reservoirs; (c) same procedure but in addition always the previous time series value is used as clue.

5.3 Replaying Soccer Games

RoboCup [67] is an international scientific robot competition in which teams of multiple robots compete against each other. Its different leagues provide many sources of robotics data that can be used for further analysis and application of machine learning. A *soccer simulation* game lasts 10 mins and is divided into 6000 time steps where the length of each cycle is 100 ms. Logfiles contain information about the game, in particular about the current positions of all players and the ball including velocity and orientation for each cycle. For our experiments we evaluated ten games of the top-five teams in a public research dataset [68] that contains recorded games from the RoboCup 2D soccer simulation league [69, 70] in 2016 and 2017 [71] (dataset available from <http://bitbucket.org/oliverobst/robocupsimdata>). We consider the (x, y) -coordinates of the ball and all 22 players for all time points during regular game play, the so-called *play-on* mode.

For LRNN learning, we use only every 10th time step of each 6000 step game with $d = 2 + 2 \cdot 22 = 46$ input dimensions and start with a reservoir consisting of $N^{\text{res}} = 500$ neurons. We repeat the learning procedure until the RMSE is smaller than 1; on average, already two attempts suffice for this. This means, if we replay the game by the learned LRNN (in output generating mode) then on average the predicted positions deviate less than 1 m from the real ones (Euclidean distance) – over the whole length of the game (cf. Figure 8 Left). Network size reduction leads to significantly less neurons compared to the original number $N = 46 + 500 = 546$ – on average 29.2% if we concentrate on the relevant components for the ball trajectory (cf. Table 3). Note that the size of the learned network is in $O(N)$ (cf. Remark 4). Thus, the LRNN model is smaller than the original time series representation of a game, which means it is substantially compressed. The complete learning procedure runs in less than a minute on standard hardware.

game	RMSE (1)	RMSE (2)	N	reduction
#1	0.00000	0.78581	385	29.5%
#2	0.00001	0.96911	403	26.2%
#3	0.00004	0.97680	390	28.6%
#4	0.00000	0.97696	406	25.6%
#5	0.00000	0.98425	437	20.0%
#6	0.00000	0.47939	354	35.2%
#7	0.00000	0.78731	390	28.6%
#8	0.00255	0.98787	385	29.5%
#9	0.00000	0.88518	342	37.4%
#10	0.00000	0.96043	376	31.1%

Table 3 For ten RoboCup simulation games, an LRNN is learned with initially $N = 500 + 46 = 546$ neurons. The table shows the RMSE (1) before and (2) after dimensionality reduction where $\theta = 1$ m. The network size can be reduced significantly – 29.2% on average (last column).

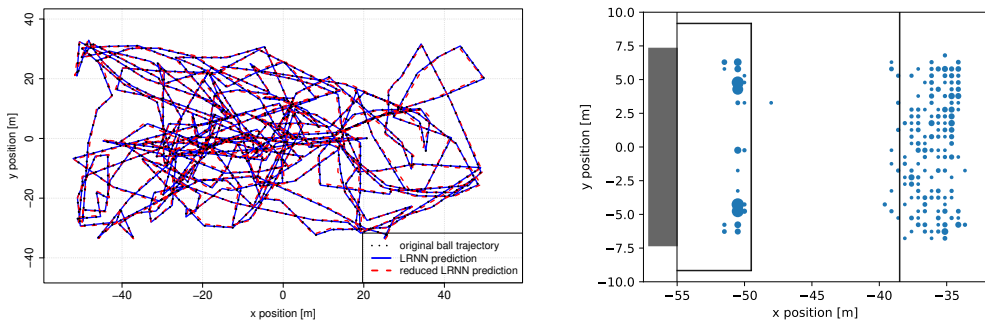


Figure 8 **Left:** Ball trajectory of RoboCup 2D soccer simulation game #6 (*Oxxy 0* versus *Gliders 2016*) on a pitch of size 105 m \times 68 m. For all 6000 time steps, the original trajectory of the ball during play is shown (dotted/black). The game can be replayed by an LRNN with $N = 500 + 46 = 546$ neurons with high accuracy (solid/blue). The reduced network with $N = 354$ reservoir neurons still mimics the trajectory with only small error (dashed/red). **Right:** Dots (in blue) mark positions that were visited more than three times (larger dots: more visits, 0.5 m resolution), information that can be derived from predictions, highlighting three larger, frequently visited regions in front of the goal.

Property 7 shows how we can learn from multiple time series at once. This is also helpful here because by this procedure we can investigate the overall behavior of a specific robot soccer agent. As example for this, we consider the trajectories of the goalkeeper of the RoboCup simulation team FRA-UNITed during the seeding and the qualifying round of RoboCup Japan Open 2020 (see <http://bit.ly/japanopen2020ssim>). For learning one LRNN from this, we employ a reservoir with $N^{\text{res}} = 1000$ neurons, adopt again a maximum threshold for the RMSE of $\theta = 1$ m, and only use every 20th step of each of the 7 games. The overall trajectory of the FRA-UNITed goalkeeper can be learned easily then (cf. Figure 8 Right). From this, one may conclude that the goalkeeper takes up three basic positions in front of the goal, does not approach the center line more than about 30 m and hardly leaves the center line.

5.4 Predicting Stock Prices

Stock price prediction is a topic that receives a considerable amount of attention in finance. Complexity of markets resulting in multiple and sudden changes in trends of stock prices make their prediction a challenge. Consequently, a number of different approaches and methods have been developed. [72] analyzes 30 different stocks by ARIMA and LRNNs using the closing stock prices 2016–2019 from <http://de.finance.yahoo.com/>. The stock price time series (consisting of 762 data points each) are split into training and testing data, with the first 80% of each series for training and the final 20% for evaluation. For a representative comparison, the RMSE of the predictions on every stock in the set is calculated. The average RMSE using LRNNs with $N^{\text{res}} = 600$ reservoir neurons is $E_{\text{test}} = 18.40$ €, lower than the average RMSE

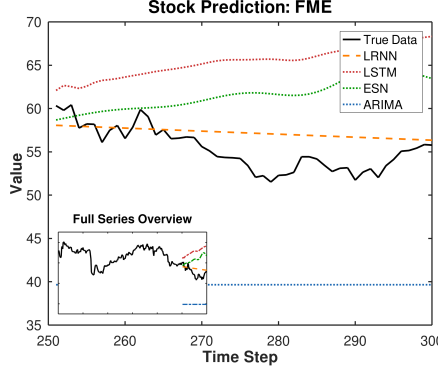


Figure 9 Stock price prediction for Fresenius Medical Care (FME.DE) with LRNNs (dashed line) and other approaches. The overall performance for all approaches often is not much better than the baseline (cf. Table 4).

using ARIMA models with seasonal patterns modeled using Fourier terms [38, p. 321] which is $E_{\text{test}} = 24.23 \text{ €}$. For shorter term predictions of 60 steps, it is possible to slightly reduce the RMSE further to $E_{\text{test}} = 17.46 \text{ €}$ by using smaller LRNNs of $N^{\text{res}} = 200$ reservoir neurons and a smaller training set of 240 data points. With an average stock price of 286.71 € of all stocks in the set, the average deviation is only 6.1%.

Apart from the good prediction results, LRNNs have the advantage that they allow the prediction of multiple stocks at the same time. An LRNN can read in 30 stocks and predict each of them concurrently. For a concurrent forecast for 60 steps, LRNNs achieve an average RMSE of $E_{\text{test}} = 30.02 \text{ €}$ with 240 training steps. Compared to ARIMA, LRNNs have also an advantage when it comes to the number of hyperparameters that have to be tuned. The LRNN model is robust when it comes to choosing the number of reservoir neurons, whereas the ARIMA model requires the adjustment of many parameters (e.g., for seasonal patterns). The compute time for ARIMA increases significantly with the number of hyperparameters. For the considered 30 stocks, LRNNs are computed about 15 times faster than the ARIMA models with the selected number of Fourier terms.

For a more systematic evaluation, we take the stocks of the German stock market index DAX (again from <http://de.finance.yahoo.com/>) and consider the last $250 + 50$ data points until the end of 2021 as training and testing data, respectively, for each stock in the DAX existing at least 300 trading days until that time. We apply the same approaches as in Section 5.1 and compute their RMSE with respect to the testing data, each normalized (i.e., divided) by the arithmetic mean of the corresponding training data. As baseline we just constantly predict the stock price of the last trading day of the training data.

As one can see in Table 4, LRNNs outperform the other approaches in the majority of all cases, namely for 19 of 39 stocks, where the resulting network size N after size reduction often is rather small. However, the overall performance for all approaches often is not much better than the baseline (see also Figure 9). In line with that, the reviews in [73, 74, 75] show that predicting stock prices remains a challenging problem, especially for a longer timeframe, which we investigate here. Contemporary research often uses complex models, ranging from LSTM RNNs [76, 77] to attention-based models with transformer architecture [66] that use further information about the events that drive the stock prices, e.g., news texts from social media [78]. These models and also LRNNs yield rather accurate results, but mainly only in the short run.

6 Conclusions

This paper presented LRNNs as an efficient and mathematically grounded approach to time series modeling. The main contribution is a closed-form learning procedure that requires solving only a linear equation system and eliminates the need for backpropagation or gradient descent. This enables fast and stable training while retaining strong approximation capabilities. LRNNs, despite using purely linear activation functions, can represent a wide class of functions,

including exponential, polynomial, and trigonometric signals. A second key contribution is the method for learning network architecture through spectral analysis of the transition matrix. This enables substantial and principled reduction in network size by identifying the most relevant dynamical modes based on eigenvalue contributions. Unlike iterative pruning, our approach reduces the network in a single step and often yields compact models with interpretable internal structure.

We have demonstrated this across several tasks, including the MSO benchmark, stock prediction, and number puzzles, where LRNNs matched or outperformed LSTMs and ESNs with significantly fewer units and faster runtime. The models also showed robustness in nonstationary and irregular data, though very large reservoirs may cause numerical issues, especially in long-term prediction. Nonetheless, the reduced models typically generalize well and support compact formula extraction for interpretable applications. These properties make LRNNs particularly suitable for domains requiring fast training, compact models, and insights into learned structure, for example, finance, embedded systems, and symbolic reasoning. Future work may explore hybrid extensions that incorporate nonlinearity or adaptive updates, while preserving the architectural simplicity and closed-form solvability of the LRNN framework.

name	DAX member stock	Baseline	ARIMA	ESN	LSTM	LRNN	
		RMSE	RMSE	RMSE	RMSE	N	RMSE
Adidas	ADS.DE	0.0554	0.0554	0.0784	0.1162	2	0.0569
Airbus	AIR.DE	0.0618	0.1070	0.0583	0.2293	2	0.0500
Allianz	ALV.DE	0.0252	0.0241	0.0199	0.0916	2	0.0503
BASF	BAS.DE	0.0438	0.0262	0.0739	0.1218	2	0.0433
Bayer	BAYN.DE	0.0414	0.0409	0.0626	0.1027	1	0.0350
BMW St	BMW.DE	0.0706	0.0706	0.0744	0.1509	11	0.0787
Brenntag	BNR.DE	0.0544	0.0938	0.0664	0.1162	2	0.0969
Continental	CON.DE	0.0518	0.0518	0.0803	0.2540	2	0.1918
Covestro	COV1.DE	0.0488	0.0488	0.0564	0.1612	1	0.0609
Deutsche Börse	DB1.DE	0.0307	0.0307	0.0249	0.0814	1	0.0347
Deutsche Bank	DBK.DE	0.0442	0.0442	0.0229	0.1794	1	0.0599
Delivery Hero	DHER.DE	0.1119	0.1040	0.1148	0.2226	3	0.0798
Deutsche Post	DPW.DE	0.0487	0.0379	0.0369	0.1822	1	0.0549
Deutsche Telekom	DTE.DE	0.0279	0.0279	0.0619	0.1209	2	0.0224
Deutsche Wohnen SE	DWNI.DE	0.2410	0.2410	0.2468	0.1706	1	0.2589
Siemens Energy	ENR.DE	0.0457	0.0457	0.0364	0.2212	9	0.0349
E.ON	EOAN.DE	0.0646	0.0646	0.0666	0.4041	1	0.0389
Fresenius Medical Care	FME.DE	0.0831	0.0842	0.0916	0.1279	1	0.0738
Fresenius	FRE.DE	0.1256	0.1256	0.1560	0.1399	2	0.1228
HeidelbergCement	HEI.DE	0.0504	0.0259	0.0708	0.1171	2	0.0912
Henkel Vz	HEN3.DE	0.0476	0.0476	0.0328	0.1479	2	0.0237
HelloFresh	HFG.DE	0.1236	0.1236	0.1241	0.3065	2	0.1220
Infineon	IFX.DE	0.1035	0.1029	0.1623	0.3574	1	0.0705
Linde PLC	LIN.DE	0.1077	0.0710	0.1134	0.1803	1	0.0909
Merck KGaA	MRK.DE	0.1293	0.0826	0.0332	0.2156	1	0.0361
MTU Aero Engines	MTX.DE	0.0598	0.0600	0.1085	0.2046	2	0.0652
Münchener Rück	MUV2.DE	0.0257	0.0256	0.0430	0.1276	1	0.0421
Porsche Vz	PAH3.DE	0.0690	0.1116	0.0920	0.1710	2	0.1188
Puma	PUM.DE	0.0894	0.0887	0.0783	0.1737	1	0.0531
Qiagen	QIA.DE	0.0660	0.0660	0.0810	0.1311	2	0.0225
RWE	RWE.DE	0.0460	0.0460	0.0805	0.1202	2	0.0276
SAP	SAP.DE	0.0398	0.0398	0.0459	0.1200	2	0.0442
Siemens Healthineers	SHL.DE	0.1057	0.0561	0.0975	0.1898	1	0.0328
Siemens	SIE.DE	0.0561	0.0354	0.0758	0.1276	2	0.0996
Sartorius Vz	SRT3.DE	0.0676	0.0676	0.0591	0.2400	1	0.0463
Symrise	SY1.DE	0.1032	0.1032	0.0893	0.1055	1	0.0755
Vonovia	VNA.DE	0.0714	0.0801	0.0662	0.1222	1	0.0593
Volkswagen Vz	VOW3.DE	0.0615	0.0615	0.1207	0.1521	2	0.1181
Zalando	ZAL.DE	0.0656	0.0656	0.1139	0.2111	2	0.0600

Table 4 Evaluation results for all stocks in the DAX existing at least 300 trading days until the end of 2021. The best performing approach is highlighted by bold face. For LRNNs, the network size N after size reduction is shown.

Acknowledgments

We would like to thank Chad Clark, Andrew Francis, Rouven Neitzel, Oliver Otto, Kai Steckhan, Flora Stolzenburg, and Ruben Zilibowitz, as well as several anonymous referees for helpful discussions and comments. The research reported in this paper has been supported by the German Academic Exchange Service (DAAD) by funds of the German Federal Ministry of Education and Research (BMBF) in the Programmes for Project-Related Personal Exchange (PPP) under grant no. 57319564 and Universities Australia (UA) in the Australia-Germany Joint Research Cooperation Scheme within the project *Deep Conceptors for Temporal Data Mining* (Decorating). A first short and preliminary version of this paper was presented at the conference *Cognitive Computing* in Hannover [79]. It received the prize for the most technologically feasible poster contribution.

References

- [1] Li Deng and Dong Yu. Deep learning: Methods and applications. *Foundations and Trends in Signal Processing*, 7(3-4):198–387, 2014. URL <http://research.microsoft.com/pubs/209355/DeepLearning-NowPublishing-Vol7-SIG-039.pdf>.
- [2] Ian Goodfellow, Yoshua Bengio, and Aaron Courville. *Deep Learning*. Adaptive Computation and Machine Learning. MIT Press, Cambridge, MA, USA, 2016. URL <http://www.deeplearningbook.org>.
- [3] Zachary C. Lipton, John Berkowitz, and Charles Elkan. A critical review of recurrent neural networks for sequence learning. CoRR – Computing Research Repository abs/1506.00019, Cornell University Library, 2015. URL <http://arxiv.org/abs/1506.00019>.
- [4] Marco Ragni and Andreas Klein. Predicting numbers: An AI approach to solving number series. In Joscha Bach and Stefan Edelkamp, editors, *KI 2011: Advances in Artificial Intelligence – Proceedings of the 34th Annual German Conference on Artificial Intelligence*, LNAI 7006, pages 255–259, Berlin, 2011. Springer. URL http://doi.org/10.1007/978-3-642-24455-1_24.
- [5] Stefan Glüge and Andreas Wendemuth. Solving number series with simple recurrent networks. In José Manuel Ferrández de Vicente, José Ramón Álvarez Sánchez, Félix de la Paz López, and F. Javier Toledo-Moreo, editors, *Natural and Artificial Models in Computation and Biology – 5th International Work-Conference on the Interplay between Natural and Artificial Computation, IWINAC 2013. Proceedings, Part I*, LNCS 7930, pages 412–420, Berlin, Heidelberg, 2013. Springer. URL http://doi.org/10.1007/978-3-642-38637-4_43.
- [6] Sepp Hochreiter and Jürgen Schmidhuber. Long short-term memory. *Neural Computation*, 9(8):1735–1780, 1997. ISSN 0899-7667. URL <http://doi.org/10.1162/neco.1997.9.8.1735>.
- [7] Albert Gu, Tri Dao, Stefano Ermon, Atri Rudra, and Christopher Ré. HiPPO: Recurrent memory with optimal polynomial projections. In H. Larochelle, M. Ranzato, R. Hadsell, M.F. Balcan, and H. Lin, editors, *Advances in Neural Information Processing Systems*, volume 33, pages 1474–1487, 2020. URL http://proceedings.neurips.cc/paper_files/paper/2020/file/102f0bb6efb3a6128a3c750dd16729be-Paper.pdf.
- [8] Albert Gu, Karan Goel, and Christopher Ré. Efficiently modeling long sequences with structured state spaces. In *The International Conference on Learning Representations (ICLR)*, 2022. URL <http://arxiv.org/abs/2111.00396>.
- [9] Zihan Wang, Fanheng Kong, Shi Feng, Ming Wang, Xiaocui Yang, Han Zhao, Daling Wang, and Yifei Zhang. Is Mamba effective for time series forecasting? *Neurocomputing*, 619:129178, 2025. ISSN 0925-2312. URL <http://doi.org/10.1016/j.neucom.2024.129178>.
- [10] Vladimir V. Klinshov, Andrey V. Kovalchuk, Igor Franović, Matjaž Perc, and Milan Svetec. Rate chaos and memory lifetime in spiking neural networks. *Chaos, Solitons & Fractals*, 158(C), 2022. URL <http://doi.org/10.1016/j.chaos.2022.112011>.
- [11] Herbert Jaeger and Harald Haas. Harnessing nonlinearity: Predicting chaotic systems and saving energy in wireless communication. *Science*, 2(304):78–80, 2004. URL

<http://doi.org/10.1126/science.1091277>.

[12] Herbert Jaeger. Echo state network. *Scholarpedia*, 2(9):2330, 2007. URL <http://doi.org/10.4249/scholarpedia.2330>.

[13] Herbert Jaeger. Controlling recurrent neural networks by conceptors. CoRR – Computing Research Repository abs/1403.3369, Cornell University Library, 2014. URL <http://arxiv.org/abs/1403.3369>.

[14] Herbert Jaeger. Using conceptors to manage neural long-term memories for temporal patterns. *Journal of Machine Learning Research*, 18(1):387–429, 2017. URL <http://dl.acm.org/doi/abs/10.5555/3122009.3122022>.

[15] Yanbo Xue, Le Yang, and Simon Haykin. Decoupled echo state networks with lateral inhibition. *Neural Networks*, 20(3):365–376, 2007. URL <http://doi.org/10.1016/j.neunet.2007.04.014>.

[16] James Martens and Ilya Sutskever. Learning recurrent neural networks with Hessian-free optimization. In *Proceedings of the 28th International Conference on Machine Learning*, pages 1033–1040, 2011. URL <http://dl.acm.org/doi/10.5555/3104482.3104612>.

[17] Peter Tiňo. Asymptotic Fisher memory of randomized linear symmetric Echo State Networks. *Neurocomputing*, 298:4–8, 2018. URL <http://doi.org/10.1016/j.neucom.2017.11.076>.

[18] Romain Couillet, Gilles Wainrib, Harry Sevi, and Hafiz Tiomoko Ali. The asymptotic performance of linear echo state neural networks. *Journal of Machine Learning Research*, 17(178):1–35, 2016. URL <http://jmlr.org/papers/v17/16-076.html>.

[19] Jeffrey L. Elman. Finding structure in time. *Cognitive Science*, 14:179–211, 1990. ISSN 0364-0213. URL http://onlinelibrary.wiley.com/doi/abs/10.1207/s15516709cog1402_1.

[20] Olivia L. White, Daniel D. Lee, and Haim Sompolinsky. Short-term memory in orthogonal neural networks. *Physical Review Letters*, 92(14):148102, 1994. URL <http://journals.aps.org/prl/abstract/10.1103/PhysRevLett.92.148102>.

[21] Yoshua Bengio, Patrice Simard, and Paolo Frasconi. Learning long-term dependencies with gradient descent is difficult. *IEEE Transactions on Neural Networks*, 5(2):157–166, 1994. ISSN 1045-9227. URL <http://doi.org/10.1109/72.279181>.

[22] Razvan Pascanu, Tomas Mikolov, and Yoshua Bengio. On the difficulty of training recurrent neural networks. *Proceedings of the 30th International Conference on Machine Learning*, 28(3):1310–1318, 2013. URL <http://proceedings.mlr.press/v28/pascanu13.pdf>.

[23] Hao Hu and Guo-Jun Qi. State-frequency memory recurrent neural networks. In Doina Precup and Yee Whye Teh, editors, *Proceedings of the 34th International Conference on Machine Learning*, volume 70 of *Proceedings of Machine Learning Research*, pages 1568–1577, Sydney, Australia, 2017. PMLR. URL <http://proceedings.mlr.press/v70/hu17c.html>.

[24] Yann Ollivier, Corentin Tallec, and Guillaume Charpiat. Training recurrent networks online without backtracking. CoRR – Computing Research Repository abs/1507.07680, Cornell University Library, 2015. URL <http://arxiv.org/abs/1507.07680>.

[25] Geoffrey Hinton. The forward-forward algorithm: Some preliminary investigations. CoRR – Computing Research Repository abs/2212.13345, Cornell University Library, 2022. URL <http://arxiv.org/abs/2212.13345>.

[26] Aaron R. Voelker, Ivana Kajić, and Chris Eliasmith. Legendre memory units: Continuous-time representation in recurrent neural networks. In *Advances in Neural Information Processing Systems 32 (NeurIPS 2019)*, Vancouver, Canada, 2019. URL <http://proceedings.neurips.cc/paper/2019/file/952285b9b7e7a1be5aa7849f32ffff05-Paper.pdf>.

[27] Antonio Carta, Alessandro Sperduti, and Davide Bacciu. Encoding-based memory for recurrent neural networks. *Neurocomputing*, 456:407–420, 2021. ISSN 0925-2312. URL <http://doi.org/10.1016/j.neucom.2021.04.051>.

[28] Antonio Orvieto, Samuel L Smith, Albert Gu, Anushan Fernando, Caglar Gulcehre, Razvan Pascanu, and Soham De. Resurrecting recurrent neural networks for long sequences. In *Proceedings of the 40th International Conference on Machine Learning*, ICML’23, pages 26670–26698, Honolulu, HI, USA, 2023. JMLR.org. URL <http://dl.acm.org/doi/abs/10.5555/3596789.3596800>.

org/doi/10.5555/3618408.3619518.

[29] Russell Reed. Pruning algorithms – a survey. *IEEE Transactions on Neural Networks*, 4(5):740–747, 1993. URL <http://ieeexplore.ieee.org/document/248452>.

[30] Namhoon Lee, Thalaiyasingam Ajanthan, and Philip H. S. Torr. SNIP: Single-shot network pruning based on connection sensitivity. In *International Conference on Learning Representations*, 2019. URL <http://arxiv.org/abs/1810.02340>.

[31] Pavlo Molchanov, Arun Mallya, Stephen Tyree, Iuri Frosio, and Jan Kautz. Importance estimation for neural network pruning. In *IEEE/CVF Conference on Computer Vision and Pattern Recognition (CVPR)*, pages 11256–11264, 2019. URL <http://doi.org/10.1109/CVPR.2019.01152>.

[32] Yitian Zhang, Liheng Ma, Antonios Valkanas, Boris N. Oreshkin, and Mark Coates. SKOLR: Structured Koopman operator linear RNN for time-series forecasting. Technical Report abs/2506.14113, Cornell University Library, 2025. URL <http://arxiv.org/abs/2506.14113>.

[33] Daniel Durstewitz. A state space approach for piecewise-linear recurrent neural networks for identifying computational dynamics from neural measurements. *PLoS Computational Biology*, 13(6):e1005542, 2017. URL <http://doi.org/10.1371/journal.pcbi.1005542>.

[34] Ting-Han Fan, Ta-Chung Chi, and Alexander Rudnicky. Advancing regular language reasoning in linear recurrent neural networks. In Kevin Duh, Helena Gomez, and Steven Bethard, editors, *Proceedings of the 2024 Conference of the North American Chapter of the Association for Computational Linguistics: Human Language Technologies (Volume 2: Short Papers)*, pages 45–53, Mexico City, Mexico, 2024. Association for Computational Linguistics. URL <http://aclanthology.org/2024.nacl-short.4/>.

[35] Hirotugu Akaike. Fitting autoregressive models for prediction. *Annals of the Institute of Statistical Mathematics*, 21(1):243–247, 1969. URL <http://link.springer.com/content/pdf/10.1007/BF02532251.pdf>.

[36] Fritz Colonius and Wolfgang Kliemann. *Dynamical Systems and Linear Algebra*, volume 158 of *Graduate Studies in Mathematics*. American Mathematical Society, Providence, Rhode Island, 2014. URL <http://doi.org/10.1090/gsm/158>.

[37] Rob J. Hyndman and Yeasmin Khandakar. Automatic time series forecasting: The forecast package for R. *Journal of Statistical Software*, 27(3), 2008. URL <http://doi.org/10.18637/jss.v027.i03>.

[38] Rob J. Hyndman and George Athanasopoulos. *Forecasting: Principles and Practices*. OTexts, Melbourne, Australia, 2013. URL <http://otexts.com/fpp2/>.

[39] J. D. Hamilton. *Time Series Analysis*. Princeton University Press, Princeton, NJ, USA, 1994. ISBN 9780691042893. URL [https://agorism.dev/book/finance/time-series/JamesDouglasHamilton-TimeSeriesAnalysis\(1994,PrincetonUniversityPress\)-libgen.lc.pdf](https://agorism.dev/book/finance/time-series/JamesDouglasHamilton-TimeSeriesAnalysis(1994,PrincetonUniversityPress)-libgen.lc.pdf).

[40] Tom Brown, Benjamin Mann, Nick Ryder, Melanie Subbiah, et al. Language models are few-shot learners. In H. Larochelle, M. Ranzato, R. Hadsell, M. F. Balcan, and H. Lin, editors, *Advances in Neural Information Processing Systems 33 (NeurIPS 2020)*, pages 1877–1901, 2020. URL <http://proceedings.neurips.cc/paper/2020/file/1457c0d6bfcb4967418bfb8ac142f64a-Paper.pdf>.

[41] OpenAI, Josh Achiam, Steven Adler, Sandhini Agarwal, Lama Ahmad, Ilge Akkaya, Florencia Leoni Aleman, Diogo Almeida, Janko Altenschmidt, Sam Altman, et al. GPT-4 technical report. Technical Report abs/2303.08774, Cornell University Library, 2024. URL <http://arxiv.org/abs/2303.08774>.

[42] Luca Pasa and Alessandro Sperduti. Pre-training of recurrent neural networks via linear autoencoders. In *Advances in Neural Information Processing Systems 27 (NIPS 2014)*, pages 3572–3580, 2014. URL <http://papers.nips.cc/paper/5271-pre-training-of-recurrent-neural-networks-via-linear-autoencoders>.

[43] Alessandro Sperduti. Exact solutions for recursive principal components analysis of sequences and trees. In Stefanos D. Kollias, Andreas Stafylopatis, Włodzisław Duch, and Erkki Oja, editors, *Artificial Neural Networks – ICANN*, pages 349–356, Berlin,

Heidelberg, 2006. Springer. ISBN 978-3-540-38627-8. URL http://link.springer.com/chapter/10.1007/11840817_37.

[44] Rudolf Kruse, Christian Borgelt, Christian Braune, Sanaz Mostaghim, and Matthias Steinbrecher. *Computational Intelligence. A Methodological Introduction*. Springer, London, 2nd edition, 2016. URL <http://link.springer.com/book/10.1007/978-1-4471-7296-3>.

[45] Steven H. Strogatz. *Nonlinear Dynamics and Chaos. With Applications to Physics, Biology, Chemistry, and Engineering*. CRC Press, Boca Raton, FL, 2nd edition, 2015. URL <http://doi.org/10.1201/9780429492563>.

[46] Roger A. Horn and Charles R. Johnson. *Matrix Analysis*. Cambridge University Press, New York, NY, 2nd edition, 2013. URL <http://www.cse.zju.edu.cn/eclass/attachments/2015-10/01-1446086008-145421.pdf>.

[47] Terence Tao, Van Vu, and Manjunath Krishnapur. Random matrices: Universality of ESDs and the circular law. *The Annals of Probability*, 38(5):2023–2065, 2010. URL <http://projecteuclid.org/euclid.aop/1282053780>.

[48] G. Manjunath and Herbert Jaeger. Echo state property linked to an input: Exploring a fundamental characteristic of recurrent neural networks. *Neural Computation*, 25(3):671–696, 2013. URL http://doi.org/10.1162/NECO_a_00411.

[49] Danil Koryakin, Johannes Lohmann, and Martin V. Butz. Balanced echo state networks. *Neural Networks*, 36:35–45, 2012. ISSN 0893-6080. URL <http://doi.org/10.1016/j.neunet.2012.08.008>.

[50] Desmond J. Higham and Nicholas J. Higham. *MatLab Guide*. Siam, Philadelphia, PA, 3rd edition, 2017. URL <http://bookstore.siam.org/ot150/>.

[51] John Wesley Eaton, David Bateman, Søren Hauberg, and Rik Wehbring. *GNU Octave – a High-Level Interactive Language for Numerical Computations*, 2017. URL <http://www.octave.org/>.

[52] Hamid Palangi, Li Deng, and Rabab K. Ward. Learning input and recurrent weight matrices in echo state networks. CoRR – Computing Research Repository abs/1311.2987, Cornell University Library, 2013. URL <http://arxiv.org/abs/1311.2987>.

[53] Michael C. Mackey and Leon Glass. Oscillation and chaos in physiological control systems. *Science*, 197(4300):287–289, 1977. URL <http://doi.org/10.1126/science.267326>.

[54] Kurt Hornik. Approximation capabilities of multilayer feedforward networks. *Neural Networks*, 4(2):251–257, 1991. ISSN 0893-6080. URL [http://doi.org/10.1016/0893-6080\(91\)90009-T](http://doi.org/10.1016/0893-6080(91)90009-T).

[55] Wolfgang Maass, Thomas Natschläger, and Henry Markram. Real-time computing without stable states: A new framework for neural computation based on perturbations. *Neural Computation*, 14(11):2531–2560, 2002. URL <http://doi.org/10.1162/089976602760407955>.

[56] Barbara Hammer. On the approximation capability of recurrent neural networks. *Neurocomputing*, 31(1-4):107–123, 2000. URL [http://doi.org/10.1016/S0925-2312\(99\)00174-5](http://doi.org/10.1016/S0925-2312(99)00174-5).

[57] Stefanie Krause, Oliver Otto, and Frieder Stolzenburg. Fast classification learning with neural networks and conceptors for speech recognition and car driving maneuvers. In Phatthanaphong Chomphuwiwat, Junmo Kim, and Pornntiwa Pawara, editors, *Proceedings of the 14th Multi-Disciplinary International Conference on Artificial Intelligence (MIWAI)*, LNAI 12832, pages 45–57, Cham, Switzerland, 2021. Springer Nature Switzerland. URL http://link.springer.com/chapter/10.1007/978-3-030-80253-0_5.

[58] Ian Jolliffe. Principal component analysis. In Miodrag Lovric, editor, *International Encyclopedia of Statistical Science*, pages 1094–1096. Springer, Berlin, Heidelberg, 2011. ISBN 978-3-642-04898-2. URL http://doi.org/10.1007/978-3-642-04898-2_455.

[59] John C. Gower and Gavin J. S. Ross. Minimum spanning trees and single linkage cluster analysis. *Journal of the Royal Statistical Society: Series C (Applied Statistics)*, 18(1):54–64, 1969. URL <http://doi.org/10.2307/2346439>.

[60] James Demmel, Ioana Dumitriu, and Olga Holtz. Fast linear algebra is stable. *Numerische Mathematik*, 108(1):59–91, 2007. ISSN 0945-3245. URL <http://doi.org/10.1007/s00211-007-0114-x>.

[61] Avrim L. Blum and Ronald L. Rivest. Training a 3-node neural network is NP-complete. *Neural Networks*, 5(1):117–127, 1992. URL [http://doi.org/10.1016/S0893-6080\(05\)80010-3](http://doi.org/10.1016/S0893-6080(05)80010-3).

[62] Jürgen Schmidhuber, Daan Wierstra, Matteo Gagliolo, and Faustino Gomez. Training recurrent networks by Evolino. *Neural Computation*, 19(3):757–779, 2007. URL <http://doi.org/10.1162/neco.2007.19.3.757>.

[63] Julien Herzen, Francesco Lässig, Samuele Giuliano Piazzetta, Thomas Neuer, Léo Tafti, Guillaume Raille, Tomas Van Pottelbergh, Marek Pasieka, Andrzej Skrodzki, Nicolas Huguenin, Maxime Dumonal, Jan Kościsz, Dennis Bader, Fréderick Gusset, Mounir Benhedi, Camila Williamson, Michal Kosinski, Matej Petrik, and Gaël Grosch. Darts: User-friendly modern machine learning for time series. *Journal of Machine Learning Research*, 23(124):1–6, 2022. URL <http://jmlr.org/papers/v23/21-1177.html>.

[64] Nathan Trouvain, Luca Pedrelli, Thanh Trung Dinh, and Xavier Hinaut. ReservoirPy: An efficient and user-friendly library to design echo state networks. In *Artificial Neural Networks and Machine Learning – ICANN 2020*, pages 494–505. Springer, Cham, Switzerland, 2020. URL http://doi.org/10.1007/978-3-030-61616-8_40.

[65] Frieder Stolzenburg. Periodicity detection by neural transformation. In Edith Van Dyck, editor, *ESCOM 2017 – 25th Anniversary Conference of the European Society for the Cognitive Sciences of Music*, pages 159–162, Ghent, Belgium, 2017. IPEM, Ghent University. URL <http://artint.hs-harz.de/fstolzenburg/papers/Sto17b.pdf>.

[66] Ashish Vaswani, Noam Shazeer, Niki Parmar, Jakob Uszkoreit, Llion Jones, Aidan N Gomez, Łukasz Kaiser, and Illia Polosukhin. Attention is all you need. *Advances in Neural Information Processing Systems*, 2017. URL <http://papers.neurips.cc/paper/7181-attention-is-all-you-need.pdf>.

[67] Hiroaki Kitano, Minoru Asada, Yasuo Kuniyoshi, Itsuki Noda, Eiichi Osawa, and Hitoshi Matsubara. RoboCup: A challenge problem for AI. *AI Magazine*, 18(1):73–85, 1997. URL <http://www.aaai.org/ojs/index.php/aimagazine/article/view/1276/1177>.

[68] Olivia Michael, Oliver Obst, Falk Schmidsberger, and Frieder Stolzenburg. RoboCup-SimData: Software and data for machine learning from RoboCup simulation league. In Dirk Holz, Katie Genter, Maarouf Saad, and Oskar von Stryk, editors, *RoboCup 2018: Robot Soccer World Cup XXII. RoboCup International Symposium*, LNAI 11374, pages 230–237, Montréal, Canada, 2019. Springer Nature Switzerland. URL http://doi.org/10.1007/978-3-030-27544-0_19.

[69] Mao Chen, Klaus Dorer, Ehsan Foroughi, Fredrick Heintz, ZhanXiang Huang, Spiros Kapetanakis, Kostas Kostiadis, Johan Kummeneje, Jan Murray, Itsuki Noda, Oliver Obst, Pat Riley, Timo Steffens, Yi Wang, and Xiang Yin. *Users Manual: RoboCup Soccer Server – for Soccer Server Version 7.07 and Later*, 2003. URL http://helios.hampshire.edu/jdavila/cs278/virtual_worlds/robocup_manual-20030211.pdf.

[70] Thomas Gabel, Egbert Falkenberg, and Eicke Godehardt. Progress in RoboCup revisited: The state of soccer simulation 2D. In Sven Behnke, Raymond Sheh, Sanem Sariel, and Daniel D. Lee, editors, *RoboCup 2016: Robot Soccer World Cup XX. RoboCup International Symposium*, volume 9776 of *Lecture Notes in Computer Science*, pages 144–156, Leipzig, 2017. Springer Nature Switzerland. URL http://doi.org/10.1007/978-3-319-68792-6_12.

[71] Olivia Michael, Oliver Obst, Falk Schmidsberger, and Frieder Stolzenburg. Analysing soccer games with clustering and conceptors. In Hidehisa Akyama, Oliver Obst, Claude Sammut, and Flavio Tonidandel, editors, *RoboCup 2017: Robot Soccer World Cup XXI. RoboCup International Symposium*, LNAI 11175, pages 120–131, Nagoya, Japan, 2018. Springer Nature Switzerland. URL http://doi.org/10.1007/978-3-030-00308-1_10.

[72] Sandra Litz. Predicting stock prices using recurrent neural networks. WAIT – Wernigeröder Automatisierungs- und Informatiktexte 01/2020, Harz University of

Applied Sciences, 2020. URL <http://doi.org/10.25673/35875>.

- [73] Dev Shah, Haruna Isah, and Farhana Zulkernine. Stock market analysis: A review and taxonomy of prediction techniques. *International Journal of Financial Studies*, 7(2), 2019. ISSN 2227-7072. URL <http://www.mdpi.com/2227-7072/7/2/26>.
- [74] Omer Berat Sezer, Mehmet Ugur Gudelek, and Ahmet Murat Ozbayoglu. Financial time series forecasting with deep learning : A systematic literature review: 2005–2019. *Applied Soft Computing*, 90:106181, 2020. ISSN 1568-4946. URL <http://doi.org/10.1016/j.asoc.2020.106181>.
- [75] Weiwei Jiang. Applications of deep learning in stock market prediction: Recent progress. *Expert Systems with Applications*, 184:115537, 2021. ISSN 0957-4174. URL <http://doi.org/10.1016/j.eswa.2021.115537>.
- [76] David M. Q. Nelson, Adriano C. M. Pereira, and Renato A. de Oliveira. Stock market's price movement prediction with LSTM neural networks. In *International Joint Conference on Neural Networks (IJCNN)*, New York, NY, USA, 2017. IEEE. URL <http://doi.org/10.1109/IJCNN.2017.7966019>.
- [77] Murtaza Roondiwala, Harshal Patel, and Shraddha Varma. Predicting stock prices using LSTM. *International Journal of Science and Research (IJSR)*, 6(4):1754–1756, 2017. URL <http://www.ijsr.net/archive/v6i4/ART20172755.pdf>.
- [78] Jintao Liu, Hongfei Lin, Xikai Liu, Bo Xu, Yuqi Ren, Yufeng Diao, and Liang Yang. Transformer-based capsule network for stock movement prediction. In *Proceedings of the First Workshop on Financial Technology and Natural Language Processing*, pages 66–73, Macao, China, 2019. URL <http://www.aclweb.org/anthology/W19-5511>.
- [79] Frieder Stolzenburg, Olivia Michael, and Oliver Obst. The power of linear recurrent neural networks. In Daniel Brunner, Herbert Jaeger, Stuart Parkin, and Gordon Pipa, editors, *Cognitive Computing – Merging Concepts with Hardware*, Hannover, 2018. URL <http://www.ai.rug.nl/minds/cogcompconf.html>.

A Proof of Property 1

For a function x and its first derivative \dot{x} with respect to time t , we have

$$\dot{x}(t) = \lim_{\tau \rightarrow 0} \frac{x(t + \tau) - x(t)}{\tau} \quad \text{and hence} \quad x(t + \tau) \approx x(t) + \tau \dot{x}(t)$$

for small time steps $\tau > 0$. We can apply this to $x^{(k)}(t)$ for $k \geq 0$ in the difference of Equation 4 between the times $t + \tau$ and t divided by τ and obtain:

$$\begin{aligned} 0 &= \frac{\sum_{k=0}^n c_k x^{(k)}(t + \tau) - \sum_{k=0}^n c_k x^{(k)}(t)}{\tau} \\ &= \sum_{k=0}^{n-1} c_k \frac{x^{(k)}(t + \tau) - x^{(k)}(t)}{\tau} + c_n \frac{x^{(n)}(t + \tau) - x^{(n)}(t)}{\tau} \\ &\approx \sum_{k=0}^{n-1} c_k x^{(k+1)}(t) + \frac{c_n}{\tau} (x^{(n)}(t + \tau) - x^{(n)}(t)) \end{aligned}$$

This is equivalent to:

$$x^{(n)}(t + \tau) \approx x^{(n)}(t) - \frac{\tau}{c_n} \sum_{k=0}^{n-1} c_k x^{(k+1)}(t)$$

From this, we can read off the desired transition matrix W of size $(n+1) \times (n+1)$ from Equation 5. Together with a start vector s satisfying Equation 4, we can thus solve differential equations approximately by LRNNs.

B Real Jordan Canonical Form

For a completely real-valued decomposition [46, Section 3.4.1], a Jordan matrix J can be transformed as follows:

1. A Jordan block with real eigenvalue λ remains as is in J .
2. For complex conjugate eigenvalue pairs $\lambda = \lambda_{\Re} + i\lambda_{\Im}$ and $\bar{\lambda} = \lambda_{\Re} - i\lambda_{\Im}$ with $\lambda_{\Re}, \lambda_{\Im} \in \mathbb{R}$, the direct sum of the two corresponding Jordan blocks $J_m(\lambda)$ and $J_m(\bar{\lambda})$ is replaced by one real Jordan block:

$$\begin{bmatrix} M & I & O & \cdots & O \\ O & M & I & \ddots & \vdots \\ \vdots & \ddots & \ddots & \ddots & O \\ \vdots & & \ddots & M & I \\ O & \cdots & \cdots & O & M \end{bmatrix}$$

$$\text{with } M = \begin{bmatrix} \lambda_{\Re} & \lambda_{\Im} \\ -\lambda_{\Im} & \lambda_{\Re} \end{bmatrix}, I = \begin{bmatrix} 1 & 0 \\ 0 & 1 \end{bmatrix}, \text{ and } O = \begin{bmatrix} 0 & 0 \\ 0 & 0 \end{bmatrix}.$$

This procedure yields a real Jordan matrix J . In consequence, we have to transform V also into a completely real-valued form. For this, for each complex conjugate eigenvalue pair λ and $\bar{\lambda}$, the corresponding eigenvectors in V can be replaced by real-valued vectors.

C Proof of Property 4

We first prove the case where the Jordan matrix J only contains ordinary Jordan blocks as in Property 2, i.e., possibly with complex eigenvalues on the diagonal. Since J is a direct sum of Jordan blocks, it suffices to consider the case where J is a single Jordan block because, as the Jordan matrix J , the matrices A and also B (see below) can be obtained as direct sums, too.

In the following, we use the column vectors $y = [y_1 \cdots y_N]^\top$ with all nonzero entries, $x = [x_1 \cdots x_N]^\top$ with $x = V^{-1} \cdot s$ (cf. Property 3), and $b = [b_1 \cdots b_N]^\top$. From b , we construct the following upper triangular Toeplitz matrix

$$B = \begin{bmatrix} b_N & \cdots & b_2 & b_1 \\ 0 & \ddots & & b_2 \\ \vdots & \ddots & \ddots & \vdots \\ 0 & \cdots & 0 & b_N \end{bmatrix}$$

which commutes with the Jordan block J [46, Section 3.2.4], i.e., it holds that (a) $J \cdot B = B \cdot J$. We define B and hence b by the equation (b) $x = B \cdot y$ which is equivalent to:

$$\begin{bmatrix} y_N & \cdots & y_2 & y_1 \\ 0 & \ddots & & y_2 \\ \vdots & \ddots & \ddots & \vdots \\ 0 & \cdots & 0 & y_N \end{bmatrix} \cdot b = \begin{bmatrix} x_1 \\ x_2 \\ \vdots \\ x_N \end{bmatrix}$$

Since the main diagonal of the left matrix contains no 0s because $y_N \neq 0$ by precondition, there always exists a solution for b [46, Section 0.9.3]. Then $A = V \cdot B$ does the job:

$$f(t) = W^t \cdot s \stackrel{\text{Property 2}}{=} V \cdot J^t \cdot V^{-1} \cdot s = V \cdot J^t \cdot x \stackrel{(b)}{=} V \cdot J^t \cdot B \cdot y \stackrel{(a)}{=} V \cdot B \cdot J^t \cdot y = A \cdot J^t \cdot y$$

The generalization to the real Jordan decomposition is straightforward by applying the fact that for complex conjugate eigenvalue pairs λ and $\bar{\lambda}$ the matrix M in a real Jordan block (cf. Section B) is similar to the diagonal matrix $D = \begin{bmatrix} \lambda & 0 \\ 0 & \bar{\lambda} \end{bmatrix}$ via $U = \begin{bmatrix} -i & -i \\ 1 & -1 \end{bmatrix}$ [46, Section 3.4.1], i.e., $M = U \cdot D \cdot U^{-1}$. The above-mentioned commutativity property (a) analogously holds for real Jordan blocks. This completes the proof.

D Proof of Property 5

Let $f_k(t)$ denote the value of the k -th dimension of $f(t)$, λ be the eigenvalue of W with maximal absolute value and m be the maximal (geometric) multiplicity of the eigenvalues of the transition matrix W . Then, from Property 2, we can easily deduce

$$|f_k(t)| = O(t^m |\lambda|^t)$$

as asymptotic behavior for large t .

E Proof of Property 8

First, we take the series of function values $f(t_0), \dots, f(t_n)$ and identify them with the time series $S(0), \dots, S(n)$. After applying the LRNN learning procedure, the LRNN runs through all given values, because by construction the upper part $[S(0) \cdots S(n-1)]$ of the matrix X (cf. Equation 10) and the matrix Y^{out} (cf. Equation 11) consist of the series of function values of f , provided that the linear matrix equation $Y^{\text{out}} = W^{\text{out}} \cdot X$ (Equation 12) has at least one solution.

Since Equation 12 is equivalent to simultaneously solving the equations $y_k = w_k \cdot X$, for $1 \leq k \leq N$ where y_1, \dots, y_N and w_1, \dots, w_N denote the row vectors of the matrices Y^{out} and W^{out} , respectively, the latter is the case if the rank of the coefficient matrix X is equal to the rank of the augmented matrix $M_k = [X \ y_k]^\top$ for every k . This leads to the equation $\text{rank}(X) = \min(N^{\text{inout}} + N^{\text{res}}, n) = \text{rank}(M_k) = \min(N^{\text{inout}} + N^{\text{res}} + 1, n)$. From this, it follows that, as desired, $N^{\text{res}} \geq n - N^{\text{inout}}$ reservoir neurons have to be employed to guarantee at least

one solution for the w_k , provided that the rank of the matrix X is maximal. For the latter, we consider two cases:

- If the rank of the upper part of the matrix X (see above) is not maximal, then this does not cause any problems. We only have to replace N^{inout} by the actual rank of the upper part of the matrix X in Equation 14.
- The rank of the lower part $[R(0) \cdots R(n-1)]$ of the matrix X almost always has maximal rank, because we employ a random reservoir (cf. Definition 3). Thus, a suitable reservoir does the job, which completes the proof.

F Solving Number Puzzles with LLMs

For comparison, we gave ChatGPT (o3) the task to solve the number puzzles from [5]. For each numbered series below the first seven terms were supplied. The value in position 8 (in parenthesis) is the ground truth next value. The tasks were (a) to predict the 8th value and (b) to give a formula that generates the entire sequence. The LLM response is shown below the series, split into next value prediction (which was correct for all 20 sequences), and a suggested generating formula (usually with alternative solutions). The predicted next values were correct for all 20 sequences, but some of the suggested generating formulas were not. Note that the LLM started indexing the values at 0.

We used the following prompt for the first sequence:

I am interested in time series prediction, and would like to see if it is possible to uncover an underlying function. I will show you the first few values, and you should (a) predict the next value, and (b) tell me the function generating the series.

Let's start with the first series:

15, 12, 8, 11, 4, 7, 0

We requested L^AT_EX output for the subsequent series (“output the formula in latex code”) that we used verbatim below. We have annotated mistakes in the formulas in red, and added remarks in orange.

Series #1 – 15, 12, 8, 11, 4, 7, 0, (3)

(a) Next value: 3.
 (b) Rule (recurrence): (incorrect formula)

$$a_0 = 15, a_1 = 12, \quad a_n = \begin{cases} a_{n-1} + 3 & n \text{ odd}, \\ a_{n-1} - 7 & n \text{ even}, n \geq 2. \end{cases}$$

Series #2 – 148, 84, 52, 36, 28, 24, 22, (21)

(a) Next value: 21.
 (b) Closed form:

$$a_n = 20 + 2^{7-n}, \quad n \geq 0.$$

Recurrence: $a_0 = 148$ and $a_n = a_{n-1} - 2^{7-n}$ for $n \geq 1$.

Series #3 – 2, 12, 21, 29, 36, 42, 47, (51)

(a) Next value: 51.
 (b) Closed form:

$$a_n = 2 + 11n - \frac{n(n+1)}{2} = 2 + \frac{n(21-n)}{2}, \quad n \geq 0.$$

Recurrence: $a_0 = 2$ and $a_{n+1} = a_n + (10 - n)$.

The alternative formulas (closed form vs recurrence) diverge for larger n but produce the same results for the first 8 relevant values of n .

Series #4 – 2, 3, 5, 9, 17, 33, 65, (129)

- (a) Next value: 129.
- (b) Closed form: $a_n = 1 + 2^n$, $n \geq 0$. (Note $a_0 = 2$.)
Recurrence: $a_{n+1} = 2a_n - 1$.

Series #5 – 2, 5, 8, 11, 14, 17, 20, (23)

- (a) Next value: 23.
- (b) Closed form: $a_n = 2 + 3n$.
Recurrence: $a_{n+1} = a_n + 3$.

Series #6 – 2, 5, 9, 19, 37, 75, 149, (299)

- (a) Next value: 299.
- (b) Closed form (**incorrect**)

$$a_n = \frac{72^n - (-1)^n}{3}, \quad n \geq 0.$$

Recurrence: (**incorrect**)
 $a_0 = 2$ and $a_{n+1} = 2a_n + (-1)^{n+1}$.

Series #7 – 25, 22, 19, 16, 13, 10, 7, (4)

- (a) Next value: 4.
- (b) Formula: $a_n = 25 - 3n$ (equivalently $a_{n+1} = a_n - 3$).

Series #8 – 28, 33, 31, 36, 34, 39, 37, (42)

- (a) Next value: 42.
- (b) Even–odd definition:

$$a_{2m} = 28 + 3m, \quad a_{2m+1} = 33 + 3m, \quad m \geq 0.$$

Single-line version:

$$a_n = 28 + 3\lfloor n/2 \rfloor + 5(n \bmod 2).$$

Series #9 – 3, 6, 12, 24, 48, 96, 192, (384)

- (a) Next value: 384.
- (b) Closed form: $a_n = 32^n$. **correct when interpreted as $3 \cdot 2^n$**
Recurrence: $a_{n+1} = 2a_n$.

Series #10 – 3, 7, 15, 31, 63, 127, 255, (511)

- (a) Next value: 511.
- (b) Closed form: $a_n = 2^{n+2} - 1$.
Recurrence: $a_{n+1} = 2a_n + 1$.

Series #11 – 4, 11, 15, 26, 41, 67, 108, (175)

(a) Next value: 175.

(b) Recurrence:

$$a_0 = 4, a_1 = 11, \quad a_{n+1} = a_n + a_{n-1} \quad (n \geq 1).$$

Closed form using Fibonacci numbers F_n ($F_0 = 0, F_1 = 1$):

$$a_n = 7F_n + 4F_{n+1}.$$

Series #12 – 5, 6, 7, 8, 10, 11, 14, (15)

(a) Next value: 15.

(b) Piece-wise form:

$$a_{2m} = 5 + \frac{m(m+3)}{2}, \quad a_{2m+1} = 6 + \frac{m(m+3)}{2}.$$

Single-line:

$$a_n = 5 + \frac{\lfloor n/2 \rfloor (\lfloor n/2 \rfloor + 3)}{2} + (n \bmod 2).$$

Series #13 – 54, 48, 42, 36, 30, 24, 18, (12)

(a) Next value: 12.

(b) Formula: $a_n = 54 - 6n$ (so $a_{n+1} = a_n - 6$).

Series #14 – 6, 8, 5, 7, 4, 6, 3, (5)

(a) Next value: 5.

(b) Recurrence:

$$a_0 = 6, \quad a_{n+1} = \begin{cases} a_n + 2 & n \text{ even}, \\ a_n - 3 & n \text{ odd}. \end{cases}$$

Closed form:

$$a_{2m} = 6 - m, \quad a_{2m+1} = 8 - m.$$

Single-line:

$$a_n = 6 - \lfloor n/2 \rfloor + 2(n \bmod 2).$$

Series #15 – 6, 9, 18, 21, 42, 45, 90, (93)

(a) Next value: 93.

(b) Recurrence:

$$a_0 = 6, \quad a_{n+1} = \begin{cases} a_n + 3 & n \text{ even}, \\ 2a_n & n \text{ odd}. \end{cases}$$

Closed form:

$$a_{2m} = 12 \cdot 2^m - 6, \quad a_{2m+1} = 12 \cdot 2^m - 3.$$

Single-line:

$$a_n = 12 \cdot 2^{\lfloor n/2 \rfloor} - 6 + 3(n \bmod 2).$$

Series #16 – 7, 10, 9, 12, 11, 14, 13, (16)

(a) Next value: 16.

(b) Recurrence:

$$a_0 = 7, \quad a_{n+1} = \begin{cases} a_n + 3 & n \text{ even}, \\ a_n - 1 & n \text{ odd}. \end{cases}$$

Closed form:

$$a_{2m} = 7 + 2m, \quad a_{2m+1} = 10 + 2m.$$

Single-line:

$$a_n = 7 + 2\lfloor n/2 \rfloor + 3(n \bmod 2).$$

Series #17 – 8, 10, 14, 18, 26, 34, 50, (66)

(a) Next value: 66.

(b) Recurrence:

$$a_0 = 8, \quad a_{n+1} = a_n + 2^{\lfloor \frac{n+3}{2} \rfloor}.$$

Closed form (even/odd):

$$a_{2m} = 3 \cdot 2^{m+1} + 2, \quad a_{2m+1} = 4 \cdot 2^{m+1} + 2.$$

Single-line:

$$a_n = 2 \left((3 + (n \bmod 2)) 2^{\lfloor n/2 \rfloor} + 1 \right).$$

Series #18 – 8, 12, 10, 16, 12, 20, 14, (24)

(a) Next value: 24.

(b) Closed form:

$$a_{2k} = 8 + 2k, \quad a_{2k+1} = 12 + 4k.$$

Single-line:

$$a_n = 8 + 2\lfloor n/2 \rfloor + (n \bmod 2)(4 + 2\lfloor n/2 \rfloor).$$

Series #19 – 8, 12, 16, 20, 24, 28, 32, (36)

(a) Next value: 36.

(b) Formula: $a_n = 8 + 4n$ (so $a_{n+1} = a_n + 4$).

Series #20 – 9, 20, 6, 17, 3, 14, 0, (11)

(a) Next value: 11.

(b) Even–odd closed form:

$$a_{2k} = 9 - 3k, \quad a_{2k+1} = 20 - 3k, \quad k \geq 0.$$

Single-line variant:

$$a_n = 9 + 11 \left\lceil \frac{n}{2} \right\rceil - 14 \left\lfloor \frac{n}{2} \right\rfloor.$$

Recurrence:

$$a_0 = 9, \quad a_{n+1} = \begin{cases} a_n + 11 & n \text{ even}, \\ a_n - 14 & n \text{ odd}. \end{cases}$$